Optimizing Recycled Bulk Molding Compound (rBMC) with Machine Learning

Luohaoran Wang

A thesis

submitted in partial fulfillment of the

requirements for the degree of

Master of Science

University of Washington

2024

Committee:

Navid Zobeiry

Benjamin Rutz

Alexander Gray

Program Authorized to Offer Degree:

Materials Science & Engineering

University of Washington

ABSTRACT

Optimizing Recycled Bulk Molding Compound (rBMC) with Machine Learning

Luohaoran Wang

Chair of the Supervisory Committee:
Navid Zobeiry, Materials Science & Engineering

Carbon fiber composites (CFCs) are important materials extensively utilized in aviation, transportation, and sporting goods industries. Carbon fiber prepreg, a precursor to CFCs, is in high demand for fabricating CFC components. A significant portion of the waste stream from producing CFCs is uncured prepreg, comprising 56-70% of the total waste generated [1]. Prepreg is a high cost, high value material, repurposing scrap and expired waste can be economically viable, in addition to being environmentally friendly. Previously, uncured prepreg has been recycled by chopping into discontinuous fiber composite (DFC), but intrinsic flaws, primarily co-location of flake ends, leads to poor properties, especially with composites thinner than 3 mm in thickness. In this work, a recycled bulk molding compound (rBMC) has been developed that mixed flakes with extra resin to improve uniformity and was processed via hot pressing to produce a defect-free composite. 0.25”-1” and 0.25-0.5" flakes showed poor dispersion. 0.25”-0.125” flakes showed exhibit good dispersion, however, the interfacial contact between fibers and resin was poor, diminishing the fibers' properties in composites. Conversely, 0.25"-0.25” flakes showed superior dispersion and mechanical properties. Gaussian Process Regression (GPR) model optimized rBMC materials based on resin content.

ACKNOWLEDGEMENT

I want to express my gratitude to my supervisors Dr. Benjamin Rutz and Dr. Navid Zobeiry, who supervised me with valuable ideas, and resources. I want to thank our research scientist Alexander Gray, who supported me with experimental techniques and professional knowledge in the experiment. In addition, I want to thank all members of UW Composites Team, especially the members from previous recycling project: Kendall Johnson, Areesa Trevino, Anita Korchemniy, Vy Huynh, for their gorgeous help and support.

Last but not the least, my sincere gratitude to my dearest families and friends, who accompany me for my life. Thanks for financial support, mental support, and inspiration.

CONTENT

1. OBJECTIVE

The objective of this work is to optimize the recycled bulk mold compound (rBMC) for manufacturability and mechanical performance, while generating a robust dataset to support commercialization. In this study, various aspects are delved, including the manufacturing process of rBMC, the characterization of impact resistance, and tensile strength of these composites.

Machine learning with Gaussian Processes Regression (GPR) techniques is aimed to analyze data obtained from different composite configurations, thereby gaining valuable insights into their performance and behavior. Furthermore, our research extends to computational modeling, building a dataset for DFC and rBMC materials.

2. INTRODUCTION

Carbon fiber reinforced polymers (CFRP) are widely used in sports, aviation, and engineering to achieve some excellent properties, such as high mechanical properties and chemical resistance [2]. The widespread use of carbon fiber results in the generation of large amounts of waste at various stages, including the production of carbon fiber (CF), prepreg, scraps, and end-of-life of manufactured components [3]. As part of carbon fiber prototypes, carbon fiber prepreg is one of the most important options for researchers. The global market for carbon fiber prepreg is expected to grow significantly due to the growing demand for composite materials. The market is projected to grow from $9.7 billion in 2022 to $18.9 billion by 2027 [4]. This growth demonstrates that the industry has recognized the benefits of carbon fiber prepreg in a variety of industries, including aerospace, automotive, wind energy, and sports

equipment [5].

It is important to consider the buy-fly ratio, which varies between 1.2:1 and 3.5:1 depending on the specific manufacturing methods. Notably, a significant portion of the waste stream consists of uncured prepreg, comprising 56-70% of the total waste generate [1]. Developing efficient strategies to manage and recycle these uncured prepreg can have a substantial impact on waste reduction and resource optimization.

The manufacture of composite components generates waste from the cutting of prepreg to achieve the desired shape and size. However, this waste can be effectively managed and reused. One approach is to reuse the excess uncured prepregs that cannot be used for their intended purpose, which offers significant environmental benefits. By recycling these materials, the industry can reduce the need for additional energy and resources to produce new material for composites, resulting in reduced carbon emissions [1, 4, 6].

Another recycling method is the chopped prepreg molding compound. This compound is applied to recycled prepreg sheets, while the remaining scraps are subjected to a shearing process to bring the flakes to the required size. The adjusted flakes are then poured into a mold and subjected to a vacuum process. Finally, the mold is cured at the desired temperature and pressure using a hot press [1].

By addressing waste management, recycling, and capitalizing on the growing market potential, the manufacturing of composite components can progress towards more sustainable practices, leading the industry towards a greener and more environmentally conscious future.

This paper introduces the recycling of prepreg cutting waste which takes a large proportion in production waste by DFC and BMC, and the construction of material database by probabilistic model GPR.

3. LITERATURE REVIEW

3.1. CARBON FIBER COMPOSITES (CFCs)

CFCs are widely used in aviation, transportation, and equipment, due to their high relative mechanical properties [2]. In carbon fiber composites, the study is focused on optimizing the manufacturing processes, enhancing the mechanical performance, and expanding the applications of carbon fiber composites [7]. Studies have delved into the fundamental understanding of the interfacial interactions between carbon fibers and matrix, seeking ways to improve the overall strength, stiffness, and durability of the composites. Additionally, there is a noTable emphasis on sustainable practices, investigating eco-friendly matrix materials and recycling methods to address the environmental impact associated with composite production [8, 9]. As one type of carbon fiber reinforced composites (CFRCs), carbon fiber polymer composites have good chemical resistance and stability [10]. Thermoset and thermoplastic composites are two distinct categories of polymer composite materials, each possessing unique characteristics and applications. Thermosets are preferred for high-performance and high-temperature applications, while thermoplastics offer advantages in terms of recyclability, impact resistance, and processing flexibility [5, 11].

CFCs in addition to polymer matrix, metal and ceramic matrixes are also used as high-performance materials by most researchers, for example, CF reinforced Al matrix

composite [12], and layered ceramic CF composite [13]. Compared with other metal-based, ceramic-based materials, polymer-based CFCs are more widely used in many applications, mainly because of their advantages of light weight, high strength, corrosion resistance, design flexibility, easy processing, and excellent thermal properties. This makes it ideal for lightweight, complex structural design, high electromagnetic performance requirements, corrosion resistance and other fields [10, 14].

3.1.1. CARBON FIBER

In general, the carbon content of CF is more than 90%, for example, the carbon content of Toray T800 is 96% [15], and the content of other parts is due to the impurities introduced in the fiber synthesis process, such as nitrogen, hydrogen, oxygen, sulfur, usually these impurities will only account for a small amount of content but they will have an impact on the mechanical and chemical properties of CF. A molecular structure of CF is shown in Figure 1, which is one type of PAN-base CF.

As the important component of CF composites, Carbon fiber serves as a structural bridge, effectively supporting the hub to facilitate load transfer and contribute to the overall stability of the structure [5]. Its significant strength-to-weight ratio ensures effective load carrying capacity, while its inherent stiffness improves structural integrity. The use of carbon fiber not only provides solid support for a hub, but also helps create a lightweight and sTable structure [16]. Except its high relative strength, carbon fiber achieves low thermal expansion coefficient. Different types of carbon fiber have different manufacturing processes and different components, so that they show different

properties and shown in Table 1.

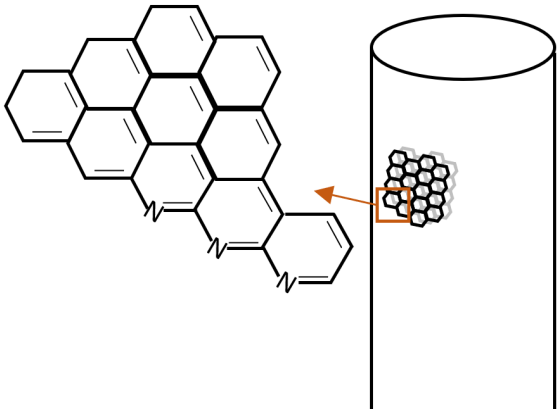

Figure 1. Molecular structure of PAN based carbon fiber [17]

Table 1. Different types of carbon fiber [18-20]

Carbon Fiber Type	Base Material	Tensile Strength GPa	Young's Modulus GPa	Final Heat Treatment Temperature
PAN-Based[1]	coal tar or petroleum pitch	3.2-6.9	240-310	Below 2000C
PAN-Based[2]	coal tar or petroleum pitch	1.9-3; 3.5-5.2	360-570; 310-350	Above 2000C
Isotropic Pitch-based[1]	polyacrylonitrile	1.1	50	Below 2000C
Isotropic Pitch-based[2]	polyacrylonitrile	0.8	60	Above 2000C
Vapor-grown	Carbon-containing gases with catalyst	3.0	240	-
Mesophase Pitch-based	from the thermal treatment of coal tar or petroleum	1.8-2.8	400-950	Above 2000C
Improved Mesophase Pitch-based	from the thermal treatment of coal tar or petroleum	2.5-3.8	320-900	Above 2000C

Where 1 and 2 mean different treatments

3.1.2. POLYMER MATRIX

Polymeric materials have become prevalent substitutes for traditional materials like metals and wood in numerous applications [21]. Two main categories of polymer

matrices are thermoplastic and thermoset. Thermoplastics have weak secondary bonds, allowing for reshaping after heating, while thermosets form permanent cross-links through curing reactions, providing high stability and durability [10]. The versatility of polymers has led to their widespread use, offering lightweight, customizable solutions in various industries.

3.1.2.1. Thermoplastic Resin

Thermoplastic resin has superior plasticity and machinability, and its molecular chain can undergo the process of heating, cooling and molding many times within a certain temperature range, forming reversible plastic deformation [22]. Compared with thermoset resin, thermoplastic resin shows higher toughness due to weak attraction between molecules. In addition, thermoplastic resins exhibit a variety of state changes at different temperatures which is clearly presented by Figure 2. At high temperature, the thermoplastic resin is liquid and the molecules have high fluidity. As the temperature drops, it may enter the glassy state, appearing as an amorphous or semi-crystalline solid structure with higher hardness. When the temperature drops further, the thermoplastic resin may enter a high elastic state, at which time it has certain fluidity and elasticity. Finally, when the temperature is raised, it may enter a viscous-flow state, and the molecules have greater mobility, making the material easy to deform [14]. This temperature-dependent state change gives thermoplastic resins plasticity and reversibility, and is suiTable for a variety of plastic processing methods, such as injection molding, extrusion and blow molding, and is widely used in the manufacture of plastic products, packaging materials and automotive parts [5, 10].

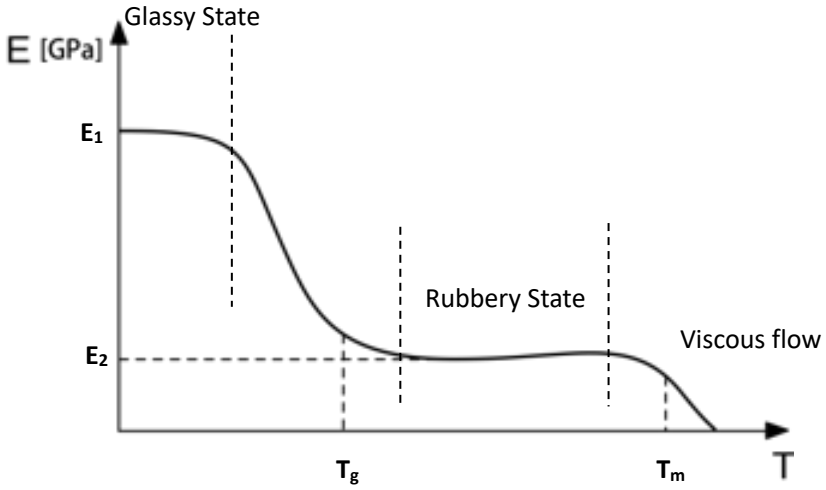

Figure 2. Glass transition temperature for thermoplastic resin

3.1.2.2. Thermoset Resin

The thermoset resin is permanently hardened and cross-linked in the process of heating and adding curing agent to form a three-dimensional network structure which shows in Figure 3 [23]. This makes thermoset resins excellent in terms of heat resistance, mechanical properties and chemical stability, which is related to the cross-linked method of thermosetting, which also makes their toughness low because the molecules are not able to move freely [10]. As an important polymer material, epoxy resin contains highly active epoxy groups in its molecular structure, which can react with curing agent to form a solid three-dimensional network structure, so that it has excellent mechanical properties, thermal stability, and chemical resistance, and has a wide range of applications in adhesives, metal coatings, aviation composite materials and other fields [5, 24]. However, due to the irreversible curing of epoxy resin, the recycling of epoxy resin is very challenging compared to the recovery of thermoplastic resin [8].

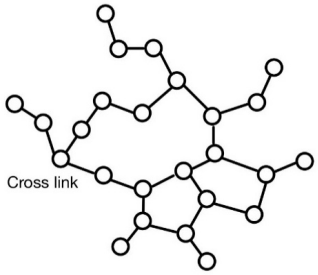

Figure 3. Thermosetting polymer structure

3.2. CARBON FIBER REINFORCED COMPOSITES RECYCLING METHODS

Sustainable development is a primary trend at present and a large amount of CF demand, recycling carbon fiber is a very hot topic which is investigated by researchers in many fields, such as mechanical engineering, aerospace engineering, and materials engineering. Due to the hardness and chemical stability of CFRPs, recycling it is a challenging task [25]. In general, recycling methods are divided into mechanical recycling, thermal recycling, and chemical recycling and shown in Figure 4, which include mechanical breakdown, thermal, and chemical degradation of resin [8]. The recyclates are classified as fibers, fillers, matrix materials, and fuels [26].

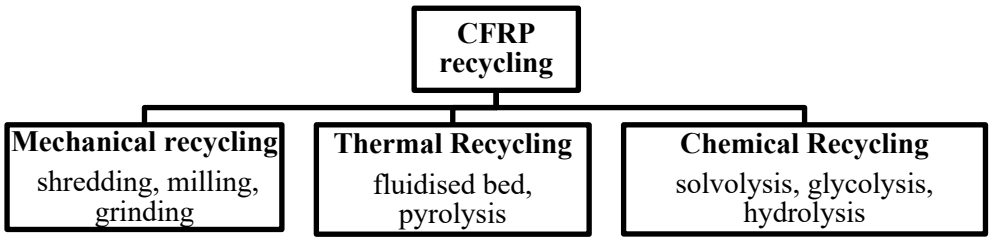

Figure 4. General methods for recycling CFRPs [8, 9]

3.2.1. Mechanical recycling

Grinding, crushing, crushing, and grinding are widely used in the recovery of CFRP, mainly to reduce the size of the refined composite material. The methods of mechanical recycling in recent years are summarized in the Table 2. According to Yang's group, the start size of scrap reduction is 50-100mm by low-speed cutting and further size is desired from 10mm to 50 microns by high-speed milling [26]. Further, some recylcates as structural fillers are added to other materials to strengthen, such as concrete, conductive plastics, and anti-static coating [27, 28].

Compared with other recycling methods, mechanical recycling is more environmentally friendly because toxic gases such as carbon monoxide cannot be produced during recycling. On the other hand, mechanical recycling is different with chemical recycling such as superfluid beds require high temperatures and pressures and thermal recycling requires high temperatures. According to Vo Dong's group, mechanical recycling approaching is closet to commercialization on industrial scale [29].

Table 2. Mechanical recycling methods for epoxy (EP)-based CFRP

Materials	Equipment	Product size
CF/EP	Rotational blade with ball milling	200 microns [30]
CF/EP	Microfine grinder drive (MF 10 basic, IKA)	25-100 microns [31]
CF/EP	HSS-PM three flute end mills	About 100-300 microns [32]

3.2.2. Thermal recycling

Thermoset composites are the most primary recycling targets because thermoplastic can be reshaped after heating. Instead, thermoset polymer molecules are linked chemically, and the cross-links are formed by curing reaction [20]. The thermal recycling methods

most focus on the recovery of fibers by oxidizing the matrix in fluidized bed and pyrolyzing at high temperature [33]. Except combustion for heat recovery, fluidized bed and pyrolysis are important methods for thermal recovery of fibers [34]. Table 3 shows some thermal recycling methods have done by researchers.

Fluidized bed technology facilitates the recycling of carbon fiber polymer composites by subjecting them to controlled thermal decomposition within a fluidized bed reactor [35]. Initially, the chopped samples are prepared by shredding, and then they are placed in the reactor filled with inert material. Hot gas or air is passed through the bed, heating composites, and causing the polymer matrix to thermally decompose into volatile gases while leaving the carbon fibers intact [35-37]. These fibers are recovered, cooled, and collected for potential reuse, while any gases produced are removed for further processing. Fluidized bed recycling is an efficient and eco-friendly method, reducing waste and the need for new carbon fiber production [38].

Pyrolysis refers to the thermal decomposition of the polymer matrix in the absence of oxygen, at high temperatures of 400 °C to 700 °C, in N_2, CO_2 or other inert environment [39]. At these elevated temperatures, the polymer matrix in the composite undergoes pyrolysis, breaking down into volatile gases such as hydrocarbons. The crucial advantage of pyrolysis is that it selectively targets the polymer while leaving the carbon fibers intact. After pyrolysis, the resulting carbon fibers are separated and can be collected for reuse in a range of applications, including aerospace, automotive, and construction [26, 35, 40].

Other pyrolysis method is relative to microwave assisted, radiation heating is replaced

traditional heating source. Heating by radiation reduces energy consumption and increases the heating rate [37]. According to Hao's group, carbon fibers were successfully extracted from CF/EP prepreg by microwave pyrolysis at temperatures of 450°C, 550°C, and 650°C. Elevated temperatures were found to have a positive impact, and carbon fibers recovered at 450°C exhibited the highest tensile strength, attributed to the protective effect of char [40].

Table 3. Thermal recycling methods for EP-based CFRP

Recycling Methods	Parameters	Remaining Strength
Pyrolysis (CF/EP) [41]	Air/N2 atmosphere 10 C/min 400C-600C 120 min	Undefined
Pyrolysis (CF/EP) [42]	N2/ 5% O2–95% N2 800C	About 80%
Pyrolysis (CF/EP) [43]	500C Remove char by oxidation in air	About 85%-90%
Fluidized bed (CF/EP) [44]	Pre-heated air: 1m/s 550C 10min	Undefined

3.2.3. Chemical recycling

Chemical recycling involves the process of chemical decomposition, depolymerization or removal of the substrate, releasing the fibers through the use of chemically dissolving reagents [38]. Waste composites are separated by dissolution with chemical solutions, such as acids and solvents. In other words, the solvent can be divided into hydrolysis, acid digestion, and glycolysis [26]. In the solvolysis method for carbon fiber recycling, a low molecular weight product is decomposed from the resin by various reactive solvents [45], for example, glycolysis and hydrogenolysis can decompose thermoset

resin into its monomers [46]. In general, solvolysis method has a wider possibilities which is relative to temperature, pressure, and other fillers [8]. Supercritical fluid has garnered significant attention in diverse fields due to their unique properties and versatile applications. A supercritical fluid exists at a temperature and pressure beyond its critical point, blurring the boundaries between gases and liquids [47, 48]. The special state combines the solvability of liquid with the diffusion ability of gas, making it an ideal medium in various processes such as extraction, particle formation and chemical reaction [49]. In recent years, researchers have explored the potential of supercritical fluids, especially carbon dioxide (SCCO2) and water (SCH2O), and used them for green, continuous and efficient extraction of bioactive compounds, pharmaceuticals and oil refining [50]. Additionally, applications in the synthesis of nanomaterials and nanocomposites have found by supercritical fluid, offering precise control over particle size and morphology [51, 52]. Moreover, supercritical fluid in catalysis, including the activation of catalysts and the design of green chemical processes, has shown great promise in advancing sustainable chemistry [8, 53].

Table 4. Chemical recycling methods for EP-based CFRP

Chemical Agents	Conditions	Remaining Strength
Macrogol 400 + Potassium hydroxide (KOH) [54]	120C-160C, 50min	99%
$AlCl_3$ + Acetic acid [55]	180C, 6h	About 97.8%
Subcritical Water [56]	260C, 105min 290C, 75min	98.2%
Super- and subcritical acetone [2]	320C, 20min	Close to 100%

3.3. DISCONTINUOUS FIBER COMPOSITE (DFC)

DFC is similar to sheet molding compound (SMC) and bulk molding compound (BMC)

are used to produce mass product of thermoset composites with small geometries as Figure 5 [57, 58]. As potential recycling methods, DFC and BMC are used for recycling typically CF prepreg. HexMC® developed a manufacturing process for DFC from prepreg flakes, which is generated by prepreg chopping, 50 mm x 8 mm flakes distributing, and rolling pressed. Nilakantan's group has investigated and presented a technique at reusing and upcycling prepreg flakes, and the effect caused by fiber orientation, flake size, and consolidation pressure, on the mechanical properties, performance, and microstructure of laminates made from the recycled scrap derived from CF/EP prepreg (Cytec CYCOM 5320 5HS) [6]. As shown in Christiane's results, the mechanical properties of DFC is lower than continuous fiber laminate about 8.02% which is due to different deformation pattern by the flake overlapping [5]. According to Johanson [7], the highest strain concentration happens at the top and end of transverse flakes which overlap with others. The initial fracture is caused because of resin-dominated properties of the transverse flakes. On the other hand, the edges of the flakes close to each other but not in contact or in tiny contact can also result in high strain concentration.

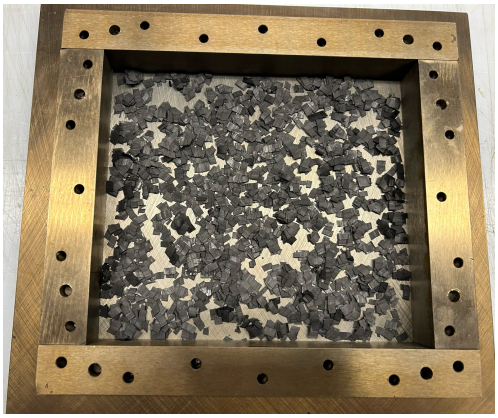

Figure 5. DFC panel manufacturing

3.4. BULK MOLDING COMPOUND (BMC)

In general, DFC and BMC contain thermoset resin and chopped fibers with other fillers to reinforce the mechanical strength, chemical stability of products [58].

BMC is a widely used class of thermoplastic composites consisting of glass fiber, filler, stabilizer, and thermoset resin (usually unsaturated polyester resin) [58-60]. The preparation process is relatively simple, by loading the mixture into a mold and pressing it at high temperatures to harden it into the desired shape. BMC stands out for its outstanding physical and mechanical properties, including high strength, stiffness, and chemical resistance. This makes BMC widely used in many fields, especially in the automotive industry, electrical equipment, and construction [57, 61]. It is widely used in the manufacture of automotive components such as car lamp shades, engine covers, and enclosures and structural parts for electrical and electronic equipment [58]. BMC not only has excellent mechanical properties, but also excellent corrosion resistance, which can maintain high performance in harsh environmental conditions. On the other hand, BMC shows a higher production efficiency, and when BMC injection molding, the cycle can be as fast as 10s/mm of part thickness [61].

Based on previous recycling methods, although there are already chemical recycling methods that can recover carbon fiber and retain almost 100% of its mechanical properties [2], most recycling methods only recover fiber and without resin [8, 62]. In the recovery of prepreg, the value of the resin often exceeds the value of the fiber. For those scraps of uncured carbon fiber prepreg that are cut in production, it is advantageous to utilize resin in the recovery of uncured prepreg [1]. The advantage of BMC is that unlike SMC, the prepreg flakes can affect their fluidity, however the

smaller objects can be more evenly distributed during hot pressing, and does not have many flakes overlapping each other like SMC [63].

Figure 6. rBMC panel manufacturing

3.5. MACHINE LEARNING

With advances in technology and algorithms, the ever-changing field of machine learning and its applications have daily changing. It has played an important breakthrough and role in the data and image processing of composite materials, such as composites manufacturing optimization [64]. The various models and algorithms that researchers are working on are mostly listed in Figure 7. These comprise supervised learning techniques like decision trees (DTs), support vector machines (SVMs), and neural networks (NNs), as well as unsupervised techniques like clustering and dimensionality reduction. Probabilistic models can also be incorporated into a variety of supervised and unsupervised learning models; these include, for supervised learning, Gaussian Process Regression (GPR), Bayesian Neural Networks (BNN), and Variational Autoencoders (VAE); for unsupervised learning, Gaussian Mixture Models (GMM) and Latent Dirichlet Allocation (LDA) [65, 66]. Lots of machine learning models are extensively used in many fields and have greatly influenced natural

language processing[67, 68].

Figure 7. Classification of machine learning models [65, 66]

3.5.1. Supervised learning

Learning process consist of training and testing steps during a simple machine learning model. After a machine model trained, defined label is output of machine learning model and the new data can be import to the model and classified by fitting data as final prediction which can be described by Figure 8. Supervised learning can provide dataset with features and labels, the inputs from features can be used to predict the labels for a model. After the algorism received correct output from relative features, the error between actual output and predicted output can be corrected by model and the model

can be self-modified [69].

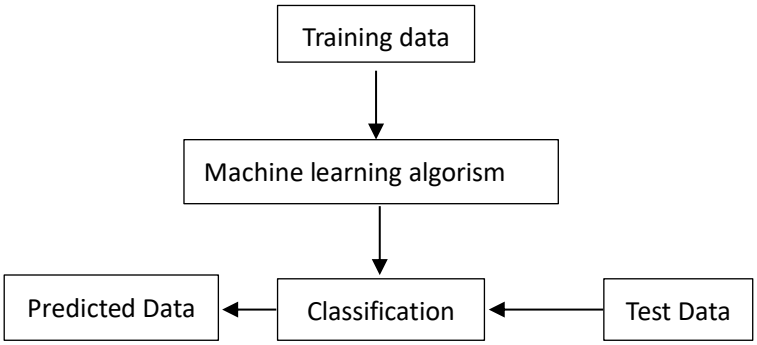

Figure 8. Schematic of supervised learning

3.5.1.1. Regression

Linear regression (LR) as a classical regression method to build and analyze the linear relationship between an independent variable and a dependent variable. LR as a simple and powerful tool that is often used to make predictions, analyze relationships between variables, and interpret trends in data [70]. Depending on the general simple LR assumption which only involved in one regressor variable, the linear relationship between independent variable and dependent variable can be described by equation 1. Multiple LR model is assumed when the number of regressor variable increase and described by equation 2 and visualized by 3D plots. Polynomial regression is a regression model can solve the relationship between variables with non-linear line which is shown by equation 3. Polynomial regression model can be considered as a specific multiple regression with higher degree variables. Polynomial regression provides the best fitting of the relationship between the dependent and independent variables. In addition, polynomial regression basically fits a wide range of curvature with board range of function [71]. Regression analysis can help confirm causality, but

it cannot be the only basis for such a claim [72].

$$y = k_0 + k_1 x + \epsilon \quad (1)$$

$$y = k_0 + k_1 x_1 + k_2 x_2 + k_3 x_3 + \cdots + k_n x_n + \epsilon \quad (2)$$

$$y = k_0 + k_1 x_1 + k_2 x_2^2 + k_3 x_3^3 + \cdots + k_n x_n^n + \epsilon \quad (3)$$

Where y is targeting vector; k0, k1…, kn are feature parameters, representing weights; x0, x1, xn are independent variables (features); ε is uncertainty.

3.5.1.2. Support Vector Machines (SVM)

SVM is used as a supervised learning algorithm for labeling objects [73]. Originally developed for binary classification, SVM has proved its versatility in handling both linear and nonlinear decision boundaries using appropriate kernel functions [74]. The basic principle of SVM is to find the hyperplane in feature space that maximally distinguishes between different classes, and the support vectors play a crucial role in defining the optimal boundary [75]. SVMs encompass a rich body of research that explores various aspects of kernel function selection, optimization techniques, and the extension of SVMs to multi-class problems. The researchers also delve into applications of the SVM in various fields, including image recognition, bioinformatics, and finance, which highlights the adaptability of the method [76].

3.5.1.3. Convolutional Neural Network (CNN)

A neural network (NN) is a mathematical or computational model that mimics the structure and function of a biological neural network (the central nervous system of an animal, especially the brain). As one type of NN models, CNN is used to process image data for object detection with three layers, convolutional layer, pooling layer, and full

connected layer. The mechanism of CNN can be described by Figure 9 [77, 78]. Convolutional layer is targeted to observe the features from pictures. Convolutional layer can be identified as a filter to recalculate the RGB matrix extracted from picture and restore in a new matrix. Because after a picture is convolved with filter, a higher dimension will be generated according to the number of convolution layers; by retaining the most significant partial output, the pooling layer ensures that no great impact is generated on the data. Full connected layers combine with all features to conclude the classification for objects. Full connected layer is a fully connected neural network, and the proportion of feedback from each neuron is different according to the weight. Finally, the classification result is obtained by adjusting the weight and network [79].

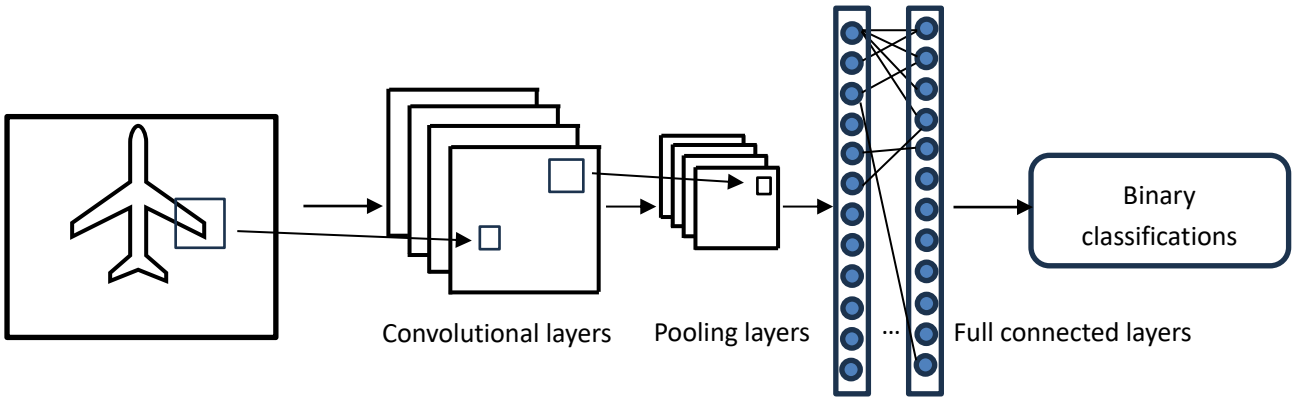

Figure 9. Schematic diagram of object detection based on CNN

3.5.2. Gaussian Process Regression (GPR)

GPR as a supervised learning model combined with probabilistic model has emerged as a powerful tool in the field of machine learning and statistical modeling [80, 81]. Originally introduced as a Bayesian non-parametric approach, GPR has found applications in diverse domains, ranging from computer science to engineering, finance,

and computing chemistry [82].

Bayesian system: Gaussian process regression has its roots in the Bayesian framework and provides a flexible, probabilistic approach to modeling complex data relationships. Researchers have extensively explored the theoretical basis of GPR, emphasizing the ability to model uncertainty and provide predictive confidence intervals. Kernel functions: The choice of kernel functions plays a decisive role in GPR. The literature emphasizes the importance of selecting an appropriate kernel to capture basic data patterns [83]. General kernels include Radial Basis Function (RBF), Rational Quadratic (RQ), and periodical (Exp) kernels, which perform specific purposes to model different types of relationships and can be performed by equation 4 to 8 [84, 85]. Different functions can be multiplied as one kernel for complex relationships.

hyperparameter adjustment: Effective hyperparameter tuning is necessary to optimize the performance of GPR models. Various approaches such as finding the best hyperparameters, cross-validation, and optimizing beige will be discussed to balance model complexity and generalizations.

$$\boldsymbol{Kernel} = C * Function \tag{4}$$

$$\boldsymbol{RBF}(\mathrm{x}, \mathrm{x}') = \sigma^2 \exp\left(-\frac{(\mathrm{x}-\mathrm{x}')^2}{2l^2}\right) \tag{5}$$

$$\boldsymbol{RQ}(\mathrm{x}, \mathrm{x}') = \sigma^2 \exp\left(-\frac{(\mathrm{x}-\mathrm{x}')^2}{2\alpha l^2}\right)^{-\alpha} \tag{6}$$

$$\boldsymbol{Exp}(\mathrm{x}, \mathrm{x}') = \sigma^2 \exp\left(-\frac{2\sin^2(\pi|\mathrm{x}-\mathrm{x}'|/p)^2}{l^2}\right) \tag{7}$$

$$\boldsymbol{Multiplying} = \boldsymbol{Function1} * \boldsymbol{Function2} + \cdots \tag{8}$$

Where C is a constant for flexibility of kernel; l is length scale for influence distance between two points; α controls the allocation of weights to different length scales

3.5.2.1. Gaussian Process (GP)

GP as a stochastic process with samples over time can be divided into Gaussian distribution (normal distribution) and random process [83]. When random variable only has one dimension, one dimension Gaussian distribution can be described by probabilistic density equation 9. GP can be defined as a random process consisting of an infinite number of Gaussian random variables on a continuous field, which is an infinite dimensional Gaussian distribution [86]. If the dimension of random variable increase to n dimension, the high dimension Gaussian distribution equation is shown as equation [87]. The description of a GP usually includes a mean function, μ and a covariance function (also known as a kernel function), Σ, which can be described by equation 10, through which the joint distribution of function values in a random process can be fully described [88].

$$p(x) = N(\mu, \sigma^2) \tag{9}$$

$$\Sigma = \mathrm{E}[(\mathrm{X} - \mu)(\mathrm{X} - \mu)^{\mathrm{T}}] = \mathrm{E}[\mathrm{X}\mathrm{X}^{\mathrm{T}}] - \mu\mu^{\mathrm{T}} \tag{10}$$

$$p(X) = N(\mu, \Sigma_{\mathrm{n}\times\mathrm{n}}) = \frac{1}{(2\pi)^{\frac{n}{2}}|\Sigma|^{\frac{1}{2}}} \exp\left(-\frac{1}{2}(X-\mu)^T\Sigma^{-1}(X-\mu)\right) \tag{11}$$

Where X is vector random variable X=[X1…Xn]$^{\mathrm{T}}$; E is average function

3.5.2.2. Bayes' Theorem (BT)

BT can be mathematically interpreted to calculate conditional probabilities [89]. In BT, an initial prior probability distribution that represents belief about the event before considering any new data. When the new data have been got, BT is used to update beliefs, getting a posterior probability distribution. This posterior distribution combines information about prior beliefs and new data. A and B events can be considered having specific beliefs. P(A|B) is the posterior probability, that is, the probability that event A

occurs after B is observed, which can be shown by equation 12. P(B|A) is the likelihood, which represents the probability that B is observed under the condition that event A occurs. P(A) is the prior probability, which is our belief in the probability of an event A before considering the new data B. P(B) is the edge likelihood, indicating the probability that B is observed under all possible A [90]. BT is widely used in the fields of statistics, machine learning and artificial intelligence. It allows to update beliefs on a rational basis, especially in small sample cases or in the face of uncertainty [91].

$$P(A|B) = \frac{P(A)*P(B|A)}{P(B)} \quad (12)$$

3.5.3. Unsupervised Learning

Unsupervised learning is a key paradigm in machine learning that has gained a lot of attention among researchers due to its ability to extract meaningful patterns and structures from unlabeled data [92]. This approach differs from supervised learning in that it does not rely on explicit labels for training. The exploration of unsupervised learning techniques covers a wide variety of applications, including clustering, dimension reduction, and generative modeling [93].

3.5.3.1. Principal component analysis (PCA)

PCA stands as a cornerstone in the field of dimensionality reduction and multivariate analysis. This technique, rooted in linear algebra, aims to capture the essential features of high-dimensional data by transforming it into a new coordinate system, where the variance along the principal components is maximized [94, 95]. PCA finds application in fields ranging from image processing and signal denoising to finance and

bioinformatics.

3.5.4. Application in Material Science

With the development of techniques and algorithms, parallel computing, numerical simulation, combined with materials science, finite element method (FEM), molecular dynamics (MD), and density functional theory (DFT) can generate many material properties [96-99]. ML can be used to predict damage, fatigue, and longevity of materials by analyzing experimental data and monitoring equipment feedback to identify possible problems with materials in advance. On the other hand, ML can optimize the preparation process of materials, improve production efficiency, and reduce costs. The algorithm can analyze the relationship between material preparation parameters and properties to help optimize the preparation process.

4. METHODOLOGY

4.1. MATERIALS

Table 5. Experimental Materials

Name	Type	Density g/cm^3	Manufacturer
Carbon fiber prepreg	T800S/3900	1.54	TORAY
YDF-173	Bis-F	1.13	Epotec
M-DIPA	Epoxy hardener	1.008	Primacure

4.2. APPARATUS

Table 6. Experimental equipment

Equipment	Manufacturer
Chopper	BOEING
Mixer	TORAY
Blue-M Oven	TPS
Hot press Machine	WABASH
Universal Test Machine (UTM)	INSTRON

Impact Tester	SATEC
Optical Microscope	OLYMPUS
Differential Scanning Calorimetry (DSC) 2500	TA
Thermogravimetric Analysis (TGA) Q50	TA
Laser LJ-X8400	KEYENCE

4.3. B-STAGE PROCESSING

B-stage preprocessing is a technique used to alleviate the challenges posed by the high viscosity of prepreg material, which can hinder cutting and lead to adherence to rollers during processing. This method involves partially curing the resin in the prepreg to reduce its tackiness and improve handling. In the described process, the prepreg was subjected to controlled heating in an oven set at 70°C for a period of 24 hours. This controlled heating partially cures the resin, modifying its properties without fully solidifying it. Consequently, the prepreg became more manageable for subsequent processing steps, facilitating easier cutting and manipulation.

Figure 10. B-staging process

4.4. DFC MANUFACTURING

The process began by cutting B-staged CF prepreg into uniform flakes using an automatic chopper which is shown in Figure 11, with lengths of 0.25 inches and 0.125 inches. A steel mold was considered to both thermal expansion of the mold and the flow dynamics of the flakes within and designed to withstand high temperatures and pressures for hot pressing. Prior to hot press, each mold component was meticulously coated with Frekote mold release agent to facilitate easy removal of the finished panel. The desired amount of CF flakes was then hand-distributed into the mold in a random fashion, ensuring homogeneity. The curing cycle was determined by DSC, the curing temperature was determined as 180C between the initial curing temperature and the fastest curing temperature. Procedure of hot press was set up with five steps. Step 1: Raise temperature to 80C without pressure; Step 2: Increase temperature to 180C with about 0.6MPa pressure; Step 3: hold for 2 hours under 0.6MPa at 180C; Step 4: Cool down to room temperature under 0.6MPa; Step 5: Release the mold from hot press. This meticulous preparation ensured the integrity and quality of the final composite product.

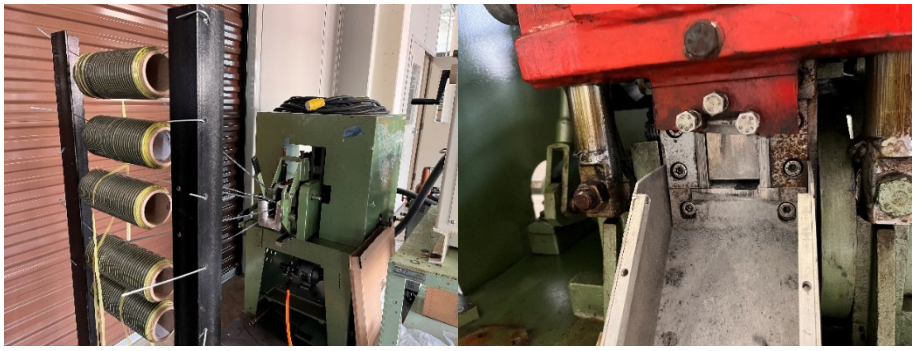

Figure 11. Chopper for prepreg flake manufacturing

Table 7. DFC manufacturing items

Sample Item	Flake Size	Thickness mm
Sample 1	0.25”-0.25”	1.0
Sample 2	0.25”-0.125”	1.0
Sample 3	0.25”-0.25”	1.6
Sample 4	0.25”-0.125”	1.6
Sample 5	0.25”-0.25”	3.2
Sample 6	0.25”-0.125”	3.2
Sample 7	0.25”-0.25”	6.4
Sample 8	0.25”-0.125”	6.4

4.4.1. Performance of DFC Panels with Intrinsic Defects

To achieve panels with thinner thickness, the panels with 0.5mm and 1.0mm thicknesses were manufactured for two sizes of flakes. The surface density of prepreg is 0.03g/cm^2, the surface area of mold is around 322.1cm^2. To fully fill a unit of surface, total weight of prepreg is 9.67g which can be calculated by equation 13. For a 0.5mm panel, about 24.8g of prepreg is required, which is obviously greater than the total mass of the required unit surface. However, the flakes were stacking on top of each other, resulting in areas where the flakes were lacking and lead to many holes on the surface.

$$W_{surface} = \rho_{prepreg} * A_{mold} = 9.67g \quad (13)$$

$$V = l_{mold} * w_{mold} * t_{panel} \quad (14)$$

Due to poor construction, 0.5mm plates cannot be investigated. After water jet cutting, most of the samples obtained in the 1.0mm panel have been damaged, as shown in the Figure 12. In addition, due to the complex topology of the panel, some of the coupons obtained from the 6.4mm panel having delamination, as shown in the Figure 13 and 14.

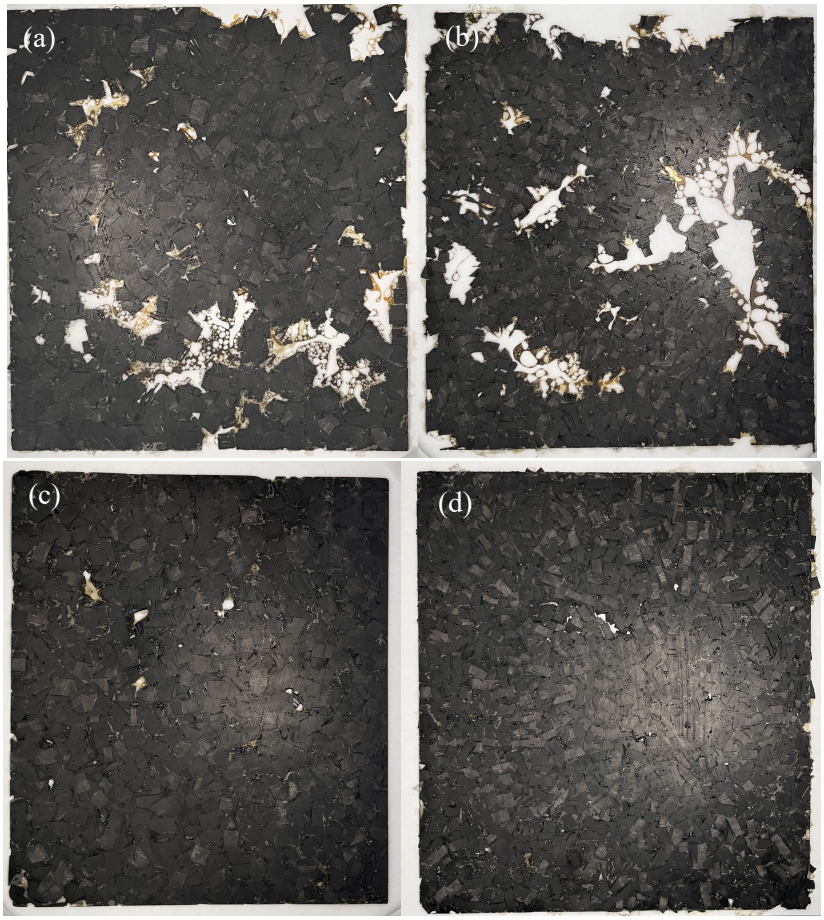

Figure 12. Performance of defective panels, (a) 0.25”-0.25” 0.5mm; (b) 0.25”-0.125” 0.5mm; (c) 0.25”-0.25” 1.0mm; (d) 0.25”-0.125” 1.0mm

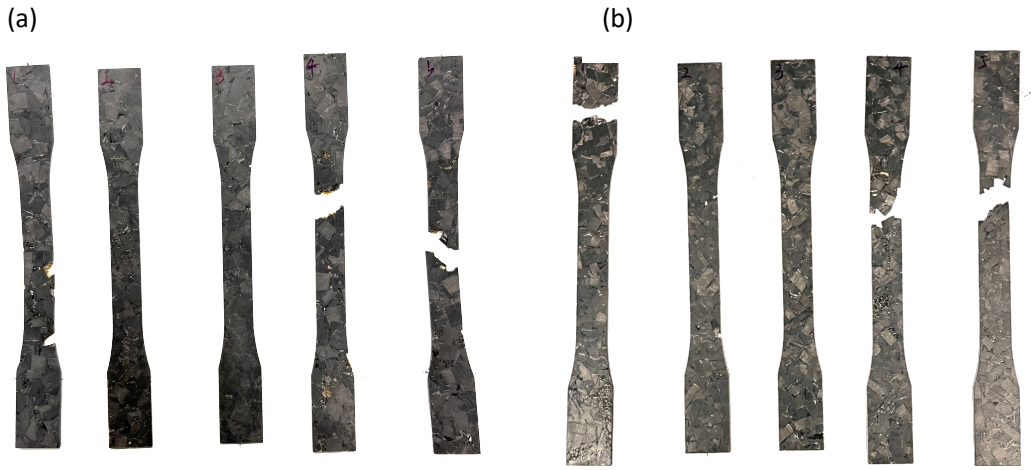

Figure 13. Performance of defective dog bones, (a) 0.25”-0.25” 0.5mm; (b) 0.25”-0.125” 0.5mm

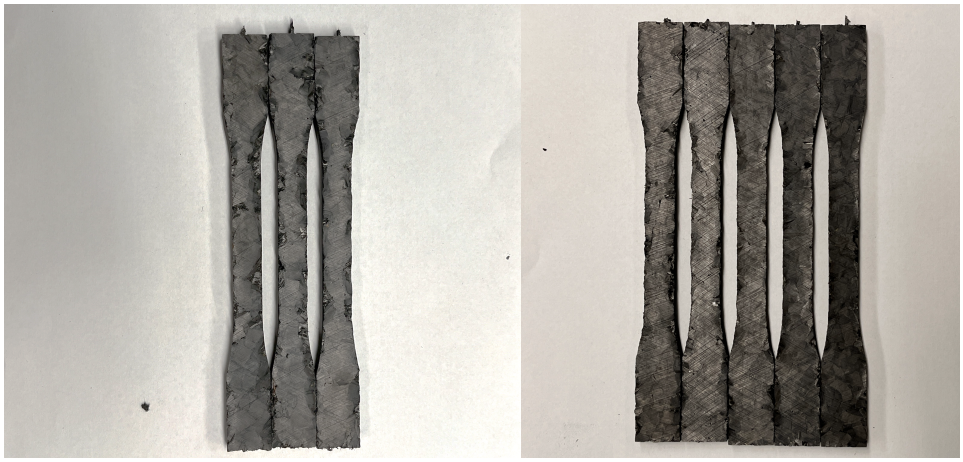

Figure 14. Performance of defective dog bones, (a) 0.25”-0.25” 6.4mm; (b) 0.25”-0.125” 6.4mm

4.5. MIXING RATIO for EPOXY SYSTEM

To calculate the mixing ratio between YDF-173 and M-DIPA, the molecular structure is shown in Figure 15. Amine equivalent weight (AHEW) of M-DIPA is calculated by Equation 15 [100], and the mixing ratio is determined by equation 17. Molecular weight (MW) of M-DIPA is 366.58 g/mol, amine value of D-PIDA is 306.07 based on Equation 16. And the AHEW can be determined and calculated as 91.645. According to datasheet of YDF-173, epoxy equivalent weight (EEW) of YDF-173 is 173, so that mixing ratio is calcuated by equation 3 and is 52.97:100 (M-DIPA:YDF-173).

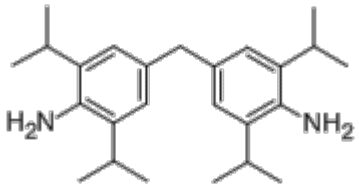

Figure 15. Molecular structure of M-DIPA

$$AHEW = \frac{56100}{Amine\ value * averge\ \#H\ per\ N} \quad (15)$$

$$Amine\ value = \frac{\#N * 5.61(MW\ KOH) * 1000\ (mg)}{Molecular\ weight\ of\ M-DIPA} \quad (16)$$

$$mixing\ ratio = \frac{AHEW}{EEW} \tag{17}$$

The density of EP-YDF-173 can be calculated by equation 18 based on the mixing ratio above. Assuming x is mass of prepreg, y is mass of resin, and φ_resin is volume fraction of resin; Based on the T-tests below, 1.6mm samples showed significant difference with 3.2mm samples and 3.2mm samples did not show significant difference with 6.4mm. To achieve lower materials with high mechanical performance, 3.2mm was setup as control thickness, depending on the current volume of mold (16.975cm x 18.975cm x 0.32cm), the volume equation and volume fraction can be described as equation 19 and 20, respectively. The volume fraction of void can be calculated from the final panels.

$$\rho_{YDF-173} * \frac{100}{100+52.97} + \rho_{M-DIPA} * \frac{52.97}{100+52.97} = 1.088 g/cm^3 \tag{18}$$

$$\frac{x}{\rho_{prepreg}} + \frac{y}{\rho_{EP-YDF-173}} = 103.072 cm^3 \tag{19}$$

$$\frac{44.81\% \frac{x}{\rho_{prepreg}} + \frac{y}{\rho_{EP-YDF-173}}}{\frac{x}{\rho_{prepreg}} + \frac{y}{\rho_{EP-YDF-173}}} = \varphi_{\text{resin}} \tag{20}$$

The resin content by weight of prepreg is 35.5%, and the resin content of volume is about 44.81%, the total content should be larger. In this experiment, the resin content is listed and show in Table 8.

Table 8. Resin content with material for BMC required

Label of BMC Panel	Volume fraction of resin	Item	Material needed grams
Panel 1	50%	Prepreg	143.80
		Resin	10.55
Panel 2	60%	Prepreg	115.04

Panel 3	70%	Resin	30.87
		Prepreg	86.28
Panel 4	80%	Resin	51.18
		Prepreg	57.52
Panel 5	90%	Resin	71.50
		Prepreg	28.76
		Resin	91.82

4.6. rBMC MANUFACTURING

rBMC was manufactured according to the steps of DFC manufacturing shown in Figure 16. The additional YDF-173 epoxy resin was added to a pile of CF flakes to achieve the recycling of CF prepreg including the epoxy resin at 80C by 30 minutes for each volume content. In order to study and optimize the performance of the panels, depending on the length of the flakes, different lengths of the flakes were used as variables for manufacturing. The primary objective was to study the dispersion dependent on the different lengths of flakes. Another variable was the volume content of the resin, using ten different volume contents of resin. After the extra resin was mixed with CF flakes, the actual weight loss of prepreg was analyzed by thermogravimetric analysis (TGA). After the release coating, the mixture was spread out by hand in the steel mold and the final panels were made by a hot-pressing machine. Four different flake sizes were considered in rBMC manufacturing and listed in table 9 and the rBMC manufacturing formula was listed in figure 17.

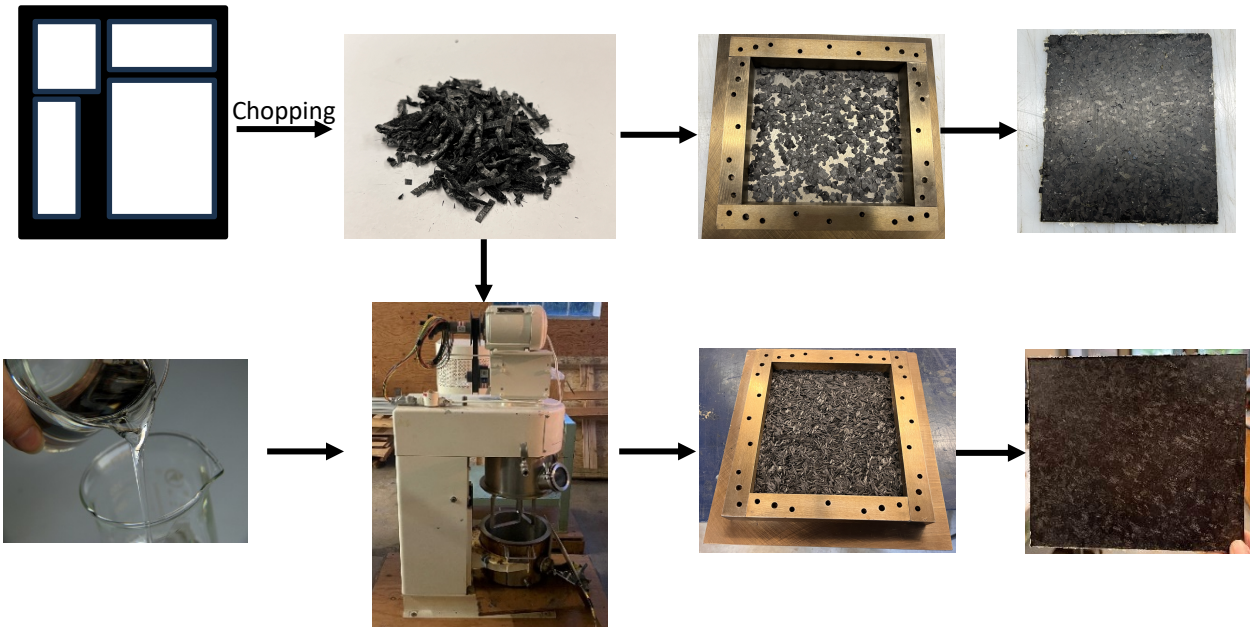

Figure 16. Manufacturing process for DFC and rBMC

Table 9. Flake sizes of prepreg

Item	Flake Size
Size 1	0.25”-1”
Size 2	0.25”-0.5”
Size 3	0.25”-0.25”
Size 4	0.25”-0.125”

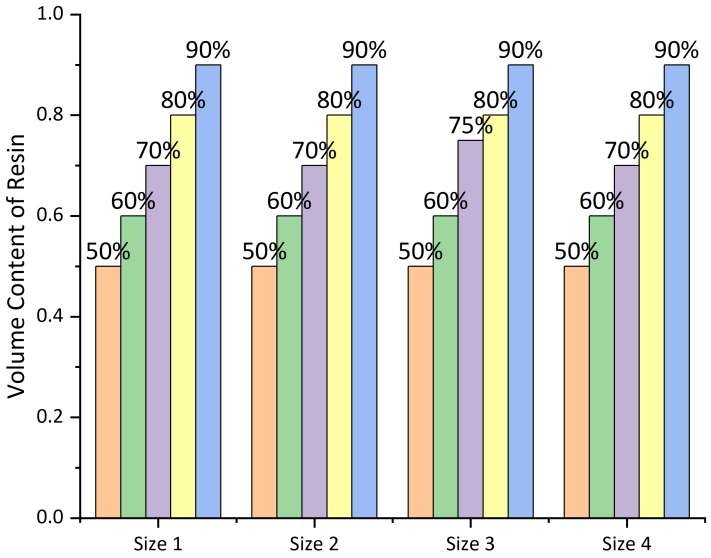

Figure 17. rBMC manufacturing formula

4.6.1. Process Induced Deformation (PID) in rBMC

Process induced deformation (PID) refers to unwanted warping or distortion of materials due to the manufacturing process. This type of deformation can be caused by a variety of sources, including thermal stress from heating and cooling cycles, mechanical stress from non-uniform forces during forming, chemical reactions that cause volume changes, and curing stress from thermosetting materials that contract or expand during curing [101].

Ideally, the fibers should be evenly distributed in the resin to maintain the structural stability and flatness of the panel. Resin-rich areas may form between the fibers for high resin content panels, and these areas may contract unevenly during curing, causing the sheet to warp [102]. PID surface plots by a laser profiler for Size 1 and Size 2 from 70% to 90% volume content of resin shown in figure 18. In Size 1 group, three panels showed warped corner. With the volume content of resin increase, PID had been partially improved, demonstrating that the internal structure can be improved at 0.25”-1” high resin content when the dispersion of the fiber was 70% uniform compared to the panel with higher volume content of resin showed PID. In Size 2 group, with the resin content increase, warping degree of panel got higher, as opposed to Size 1 when the structures of flakes were also not decomposed when dispersed, possibly because the longer fibers tend to span the voidage and disperse the stress more efficiently in the composites, potentially leading to better stability and less warping under thermal and mechanical stresses. Compared to other groups, the shorter flakes were able to be broken down during mixing so that no significant warping occurred.

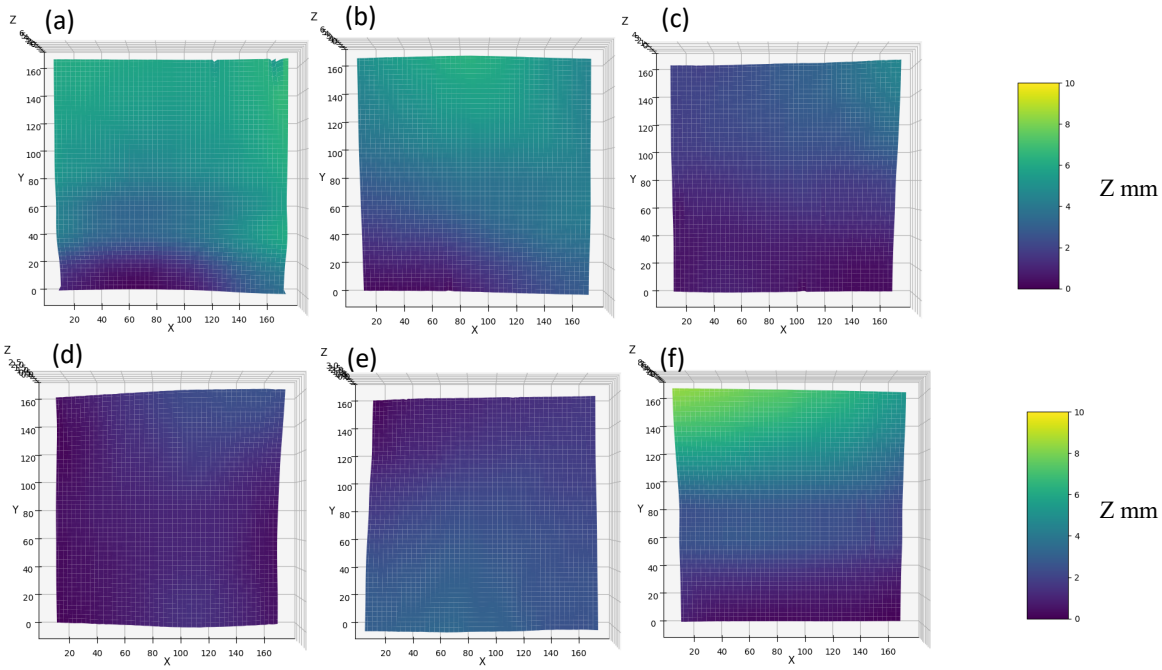

Figure 18. PID surface plots for 0.25”-1” (a), (b), (c); 0.25”-0.5” (d), (e), (f) from 70% to 90% volume content of resin, respectively

5. CHARACTERIZATION

5.1. DIFFERENTIAL SCANNING CALORIMETRY (DSC)

Curing kinetics study of the epoxy resin system was conducted by DSC 2500. About 7 mg of three types of materials were sealed in TA aluminum hermetic pan, including virgin prepreg, B-staged prepreg, and EP-YDF-173 resin. The temperature range of ramp was set from -50C to 350C with 10C/min heating rate.

Figure 19. DSC 2500 from TA

5.2. TENSILE TEST (DIC)

The tensile test was conducted using a universal testing machine (UTM) INSTRON-5585H model with the maximum 250 kN load capability. The dimensions of dog bone are following type I and cut by waterjet, and the loading rate of the upper crosshead was set as 0.5 mm/minute, which referred to the ASTM D638 standard [103]. The stress versus strain data were obtained by Bluehill software. The wedge grips combined with polishing paper were strongly tied between the specimen and clamp device. STF camera was used to record and perform the DIC analysis procedure during tensile test. Figure 18 illustrates the experimental setup of the tensile test.

Figure 20. Tensile test with DIC setup

5.3. IZOD IMPACT TEST

The Izod test was conducted by SATEC impact tester. The Izod tests were investigated with 2.7J capability and following ASTM D4812. Unnotched specimens with different thickness were used to record the impact resistance.

Figure 21. Pendulum type Impact tester

5.4. THERMOGRAVIMETRIC ANALYSIS (TGA)

Actual volume content of resin was investigated by TGA Q50. The TGA samples were cut into small flakes using scissors around 10mg and the samples were placed on a platinum pan. The recipe was setup with two stages: Stage 1: Ramp from room temperature to 500C with 10C/min and hold for 20min under nitrogen environment; Stage 2: Ramp from 500C to 550C with 10C/min and hold for 90min under air environment [104].

Figure 22. TGA Q50 from TA

5.5. OPTICAL MICROSCOPE

To investigate the cross section of failure coupons from IZOD test, OLYMPUS BX-UCB optical microscope was used to detect the cross-section structure of tested coupon. UMPlanFI-5X/0.15 and UPlanFL-N-10X/0.3 lenses were using for microscopy.

Figure 23. Olympus optical microscope

6. RESULT ANALYSIS & DISCUSSION

6.1. PART 1: DFC

6.1.1. Differential Scanning Calorimetry (DSC)

To investigate the curing temperature of virgin and B-staged prepreg thermal reaction process was conducted by DSC. Compared to virgin and b-staged prepreg presented by Figure 24, the glass temperature of b-staged material showed increase around 44C depending on the first endothermic peak. The curing cycle of b-staged prepreg started from 162C and had the peak curing rate around 250C. Compared to the exothermic peaks of B-staged prepreg and virgin prepreg, the curing cycle started earlier than virgin prepreg. Except the endothermic peak, the general shapes of two materials were similar. In addition, after curing cycle, b-staged prepreg showed an earlier rapid energy absorption which could be caused by less thermal stability compared to virgin prepreg. Enthalpy change of virgin prepreg was 17.87 and 25.74 W*C/g for B-staged prepreg, respectively. Degree of cure (DOC) could be calculated by equation and DOC was about 0.31.

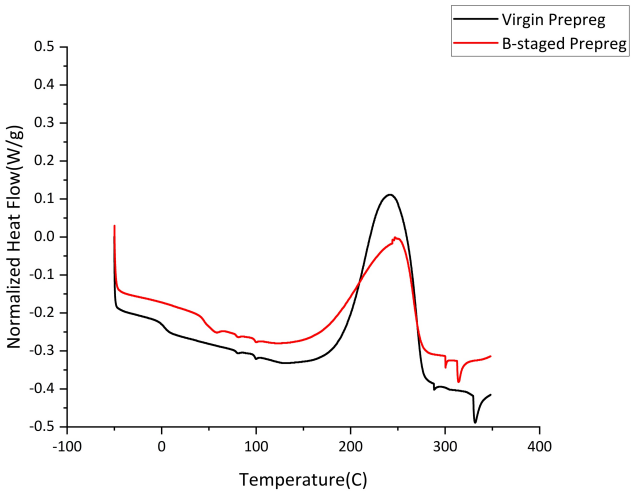

Figure 24. Heat flow curve from DSC for virgin and B-staged prepreg

$$DOC = \frac{H_{residual}}{H_{total} - H_{residual}} \tag{21}$$

6.1.2. Tensile Test with Digital image correlation (DIC)

Table 10 clearly showed the tensile strength of four different panel thicknesses with two different flake sizes. The Sample 5 showed the highest tensile strength about 63.18 ± 8.51 MPa. The specimen with the best tensile strength, which was about 55.11MPa higher than the lowest tensile strength. The T-test was conducted for each thickness group, and the P-value was higher than the critical value of 0.05. There were no significant differences in the tensile strength of the template of 1mm&1.6mm and 3.2mm&6.4mm groups. Figure 25 clearly showed the tensile strength for each panel with error bar. In general, the longer flake length was, the better the tensile strength was, and the average tensile strength was about 15.7% higher than that of the shorter flake length**.** The transverse strength in the flakes was significantly less than the longitudinal strength, while the strength of the transverse flake was generally considered to be lower than the strength of the matrix material [105]. In this case, when the longitudinal flake tips are alternately in contact with the transverse flake, cracks develop in this area,

which is due to the load transfer of the longitudinal bundle to the transverse bundle, resulting in a crack near the transverse flake. Primary strain concentration is caused around the flake tips and heavily impacted by the structure of underlying flakes [106]. For square flakes, although the direction of the fibers cannot be distinguished by the naked eye, usually high strain concentrations occur in areas where the tips of the longitudinal flake are in contact with the non-longitudinal bundle, or where the edges of the flake are close together but not bonded. It is worth noting that the formation of cracks is also related to the presence of pores in the composites [107]. However, the panel with 1.6mm thickness showed the panel with Size 4 flake had a better tensile strength around 27.0% higher than 0.25"-0.25" one. In 1.0mm group, Size 3 panel performed a wider error bar, which had the lowest tensile strength close to 0 MPa.

Figure 26 presented the tested coupon from Sample 1 with DIC diagram of strain concentration. Some of notches were significant performed on the surface which was caused by lack of resin and the inhomogeneous distribution of flakes in the mold during hot press. The crack initiation happened at the co-location of flake-ends and poor resin region, which were labelled by orange circles on the diagram. The extension of the crack avoided the longitudinal fiber and spread along the transverse fiber direction. Low strain concentration happened on the coupon surface which located with transverse flakes and closed to transverse flakes. Depending on the concentration of strain, the orientation of flake could be roughly identified and the macroscopic surface structure of the composite was observed by mobile phone microscope and presented by Figure 25, which clearly showed fracture happened at position of transverse flakes and Figure

27 (a) pointed flake stranded out from coupon. Poor resin region and rich resin region were caused by the intrinsic flaws that the gap between the ends of discontinuous flakes, which were clearly shown in Figure 27 (c) and (d) and led to the low strain concentration happened. For these thinner coupons, the crack initiation could be generated around the holes or cracked edges. As a DFC coupon, the tensile failure of this coupon could be clearly identified as matrix failure and sliding of fracture surface due to interlaminar failure [108].

Table 10. Tensile strength for different thickness with two sizes of flake

Sample Item	Tensile Strength MPa	±Std
Sample 1	10.03	9.27
Sample 2	8.07	3.69
Sample 3	38.69	7.92
Sample 4	49.12	9.21
Sample 5	63.18	8.51
Sample 6	56.19	4.26
Sample 7	59.16	9.45
Sample 8	49.37	12.74

Table 11. T-test for thickness groups

Thickness	Flake Size	t value	p value	Explanation
1&1.6	Size 3	-1.88	0.20	Not Significant
	Size 4	-4.17	0.05	Not Significant
1&3.2	Size 3	-4.78	0.04	Significant
	Size 4	-12.46	0.01	Significant
1&6.4	Size 3	-5.67	0.03	Significant
	Size 4	-9.91	0.01	Significant
1.6&3.2	Size 3	-4.21	0.00	Significant
	Size 4	-1.39	0.20	Not Significant
1.6&6.4	Size 3	-3.32	0.01	Significant
	Size 4	-0.03	0.98	Not Significant
3.2&6.4	Size 3	0.63	0.55	Not Significant
	Size 4	1.02	0.34	Not Significant

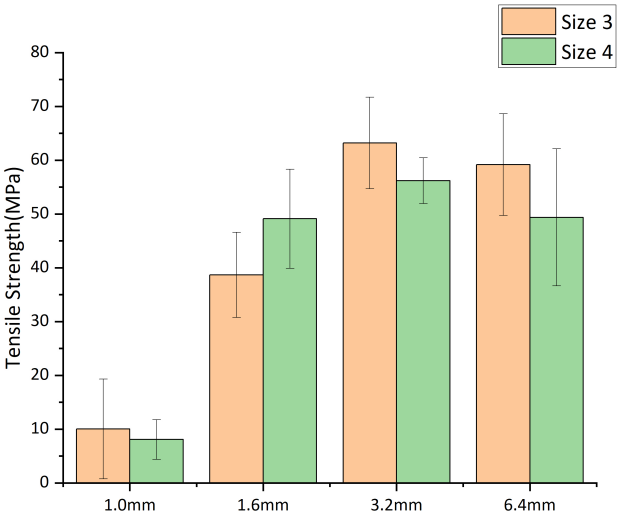

Figure 25. Tensile strength of DFC panels under four thicknesses

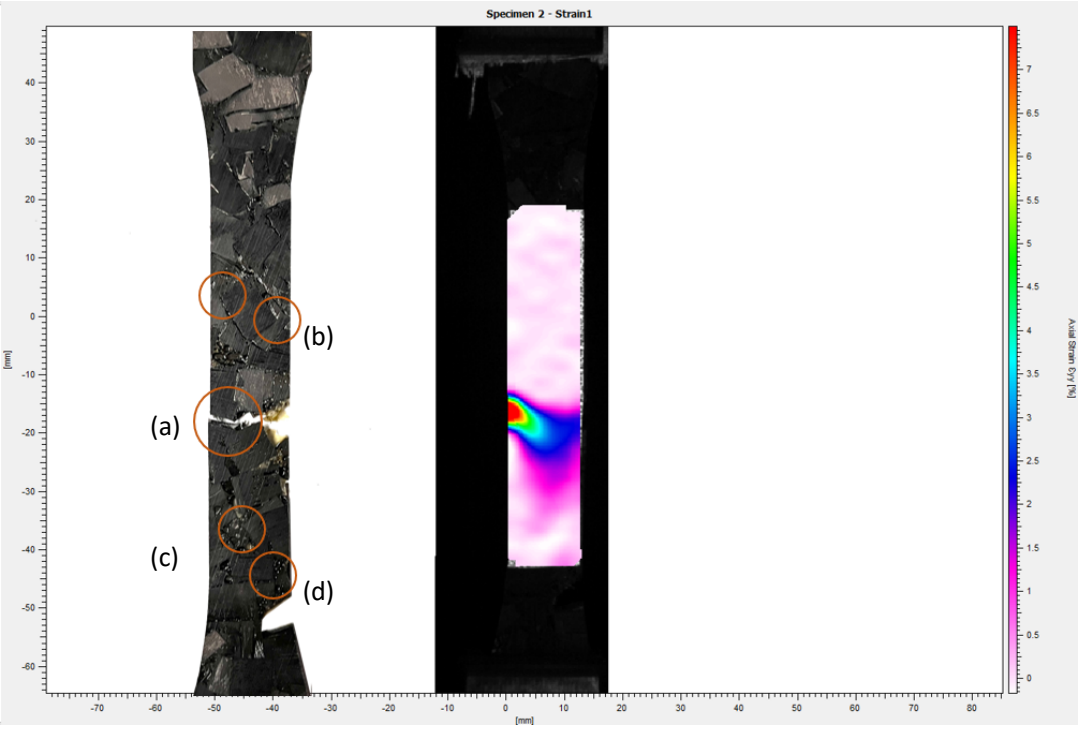

Figure 26. DIC comparison for coupon from Sample 1

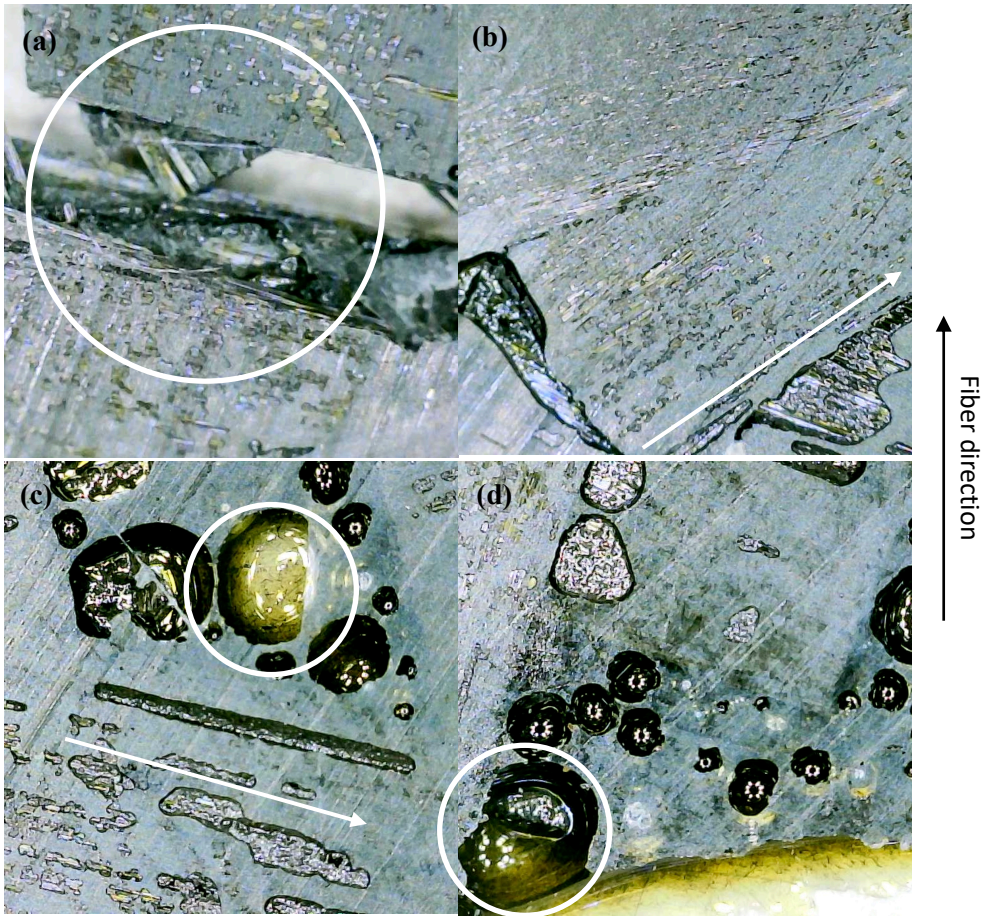

Figure 27. Macro surface of coupon by Digital microscope

6.1.2.1. Convolutional Neural Network Model Based on Digital Image Correlation

To process the image data from DIC, object detection could be performed by CNN model. The model, SSD ResNet50 V1 FPN 640x640 (RetinaNet50) pre-trained on the 2017 COCO dataset, was introduced which is from TensorFlow 2 Detection Model Zoo, Github open source. As a compositing object detection model, Single Shot Multibox Detector (SSD) uses multi-scale feature maps to predict bounding boxes so that objects of different sizes can be captured [109]; Resnet50 as one of residual network families can be a feature extractor and eliminate the problem of gradient disappearance; Feature Pyramid Network (FPN) is a technique used to enhance the feature hierarchy of convolutional networks, especially for scale change problems in object detection tasks [110].

I. Image Collection and Processing

After tensile tests, the videos including change in strain concentration with time were exported. To observe single frame from tensile test video, Open AI as a powerful image processing repository was used to extract images with cropped detecting area. Labelme as an open-source image labeling tool was aimed to annotate personalized features, Non-crack (NC), Low-strain concentration (LSC), and Crack Initiation (CI).

Figure 28. Process of crack detection by CNN

II. Results and Discussion

Figure 29 (a) showed the application of a CNN in detecting areas of non-crack area (NC), crack initiation (CI) and low strain concentration (LSC) that indicate potential cracks in DFC specimen. (b) Learning rate decreases over time, suggesting that the model is continuously improving its accuracy, preventing overfitting and ensuring more accurate crack detection; (c): The stability of the computational performance as reflected in the number of steps per second indicates that the CNN is processing the data efficiently, which is critical for applications that require real-time analysis; (d): The decrease in total loss indicates good learning, as the model quickly masters the necessary features for crack detection and gradually increases its sensitivity to subtle signs of material failure.

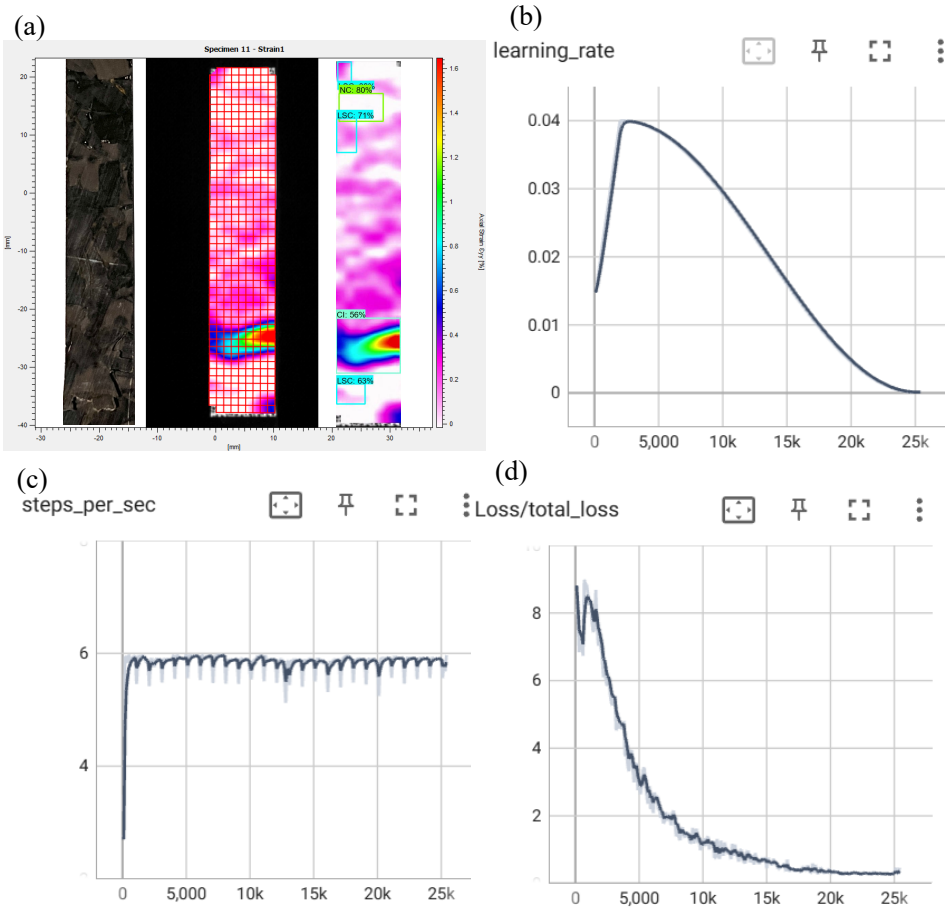

Figure 29. CNN results (a) Detected example; (b) trend of learning rate; (c) step rate; (d) Total loss of training model

III. Application

The trained CNN model, leveraging an accurate dataset, can be integrated into Python code for an add-in designed to detect crack initiation during single tensile tests. This model is applicable to various loading structures for monitoring cracks and detecting failures. Given the complex intrinsic structures of DFC materials, it is possible to configure unique features within the model to specifically analyze and predict their unique failure mechanisms. This automated detection is crucial for identifying weak points in materials before they lead to failure, enhancing safety and reliability in material-intensive industries like aerospace and construction.

6.1.2.2. Regression Analysis

To investigate the relationship between tensile strength and the thickness of panel, three regression methods were used, linear regression, polynomial regression, and Gaussian Process regression (GPR). According to Table 12, the observed dataset cannot fit on the linear curve well with smaller R^2 which means linear regression only shows small correlation. Compared polynomial regression results to linear regression results, the observed data fairly fitted on the polynomial curve especially the third polynomial regression, which had higher R^2. Although R^2 were 1 from the third polynomial curves, curves fitted with very few data points resulting in overfitting. Compared to these results, the secondary polynomial regression for 0.25" flake length performed higher correlation in these groups. GPR with four different kernels was applied and shown in Figure 30 and functions are shown by equation 21 to 24, all show the prediction trend with 95% confidence boundaries. Combined with the predicted results from different kernels, there was a maximum tensile strength between the thickness of 3 and 6mm, also based on defects that occur during processing at 6.4mm.

Table 12. Regression results

Regression Method	R^2 for Size 3	R^2 for Size 4
Linear	0.53	0.27
Secondary Polynomial	0.95	0.74
Third Polynomial	1.00	1.00

$$Kernel\ 1: C * RBF(1, (1e^{-3}, 2)) \quad (22)$$

$$Kernel\ 2: C * RQ(l = 1, \alpha = 0.2) \quad (23)$$

$$Kernel\ 3: C * Exp(l = 1, p = 1) * RQ(l = 1, \alpha = 0.2) \quad (24)$$

$$Kernel\ 4: C * RBF * RQ + Exp * RQ \quad (25)$$

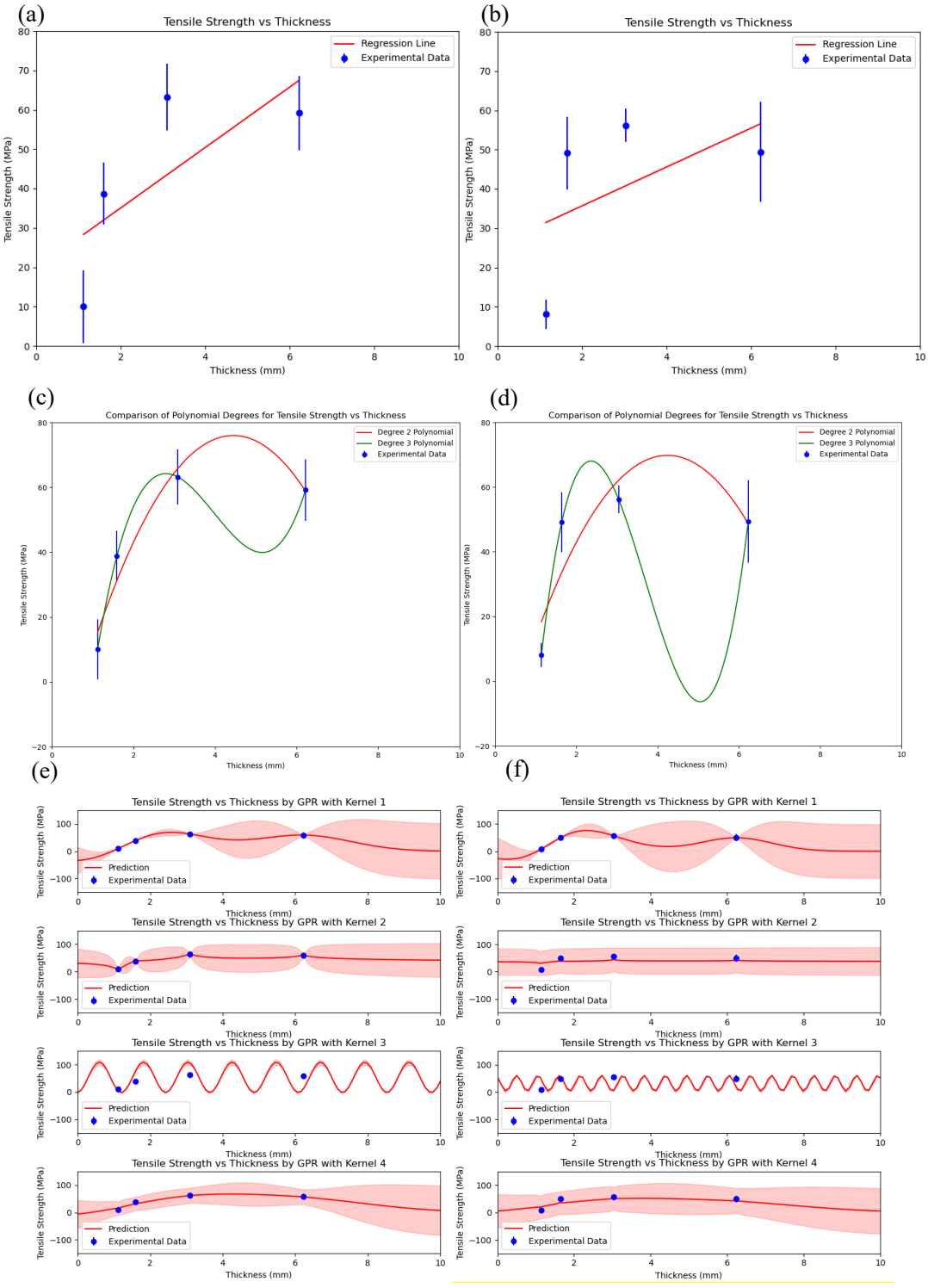

Figure 30. Different Regression results for two sizes of flakes

6.1.3. IZOD Test

The results of fracture energy were shown in Table 13 and analyzed by t-test. According to the Table 14, Sample 7 had the highest absorbed energy which is 32.93 ± 2.83 KJ/m^2 and higher about 77.7% than the lowest one. Compared to each group with two flake

sizes, longer fiber length with higher thickness showed higher impact resistance. In general, long carbon fibers are generally able to transfer loads more efficiently and withstand more internal stress than short carbon fibers because of their continuity, enhanced mechanical properties, directivity, and properties that prevent crack propagation [10, 111]. However, Sample 2 had better impact energy absorption about 2 KJ/m^2 higher than Sample 1. The comparison in failure types of coupons could be concluded by Figure 32. For thinner thicknesses of coupon as 1.0mm and 1.6mm were all completed break. For 3.2mm, coupon from Sample 5 performed better impact resistance than Sample 6 coupon with partial break and all 6.4mm thickness coupons showed partial break. According to Seunghyun Ko, etc. work, DFC is highly impacted by its thickness structure especially from 1.65mm to 3.75mm which shows a modulus increase with a normal distribution and strength increase with Weibull distribution [4]. From t-test analysis, except the group of 3.2mm&6.4mm, other groups had the differences were significant. The possible reason could be caused by random distribution of flakes with complex structure. Depending on Figure 31, each sample presented wider error bar especially Sample 5, which shows 43.7% higher or lower based on the mean fracture energy. As DFC materials, the random interlaminar structure impacted its mechanical properties which could be classified as underlying flake architecture and inhomogeneous distribution.

Table 13. IZOD test results for DFC

Sample Item	Cross-section area e-5 m^2	±std e-7	Fracture Energy KJ/m^2	±std	Failure Type
Sample 1	1.43	7.08	7.75	3.47	C
Sample 2	1.41	2.67	9.72	4.36	C
Sample 3	1.87	12.56	16.81	3.59	C
Sample 4	1.93	14.94	7.35	2.19	C
Sample 5	3.67	27.13	25.31	14.24	P
Sample 6	3.60	29.57	18.24	6.64	C
Sample 7	7.64	40.81	32.93	2.83	P
Sample 8	7.44	49.51	28.47	4.83	P

Where C is completed break; P is partial break

Table 14. T-test for thickness groups

Group of Thickness	Flake Size	t value	p value	Explanation
1&1.6	Size 3	-3.71	0.00	Significant
	Size 4	1.08	0.30	Not significant
1&3.2	Size 3	-2.61	0.03	Significant
	Size 4	-3.00	0.02	Significant
1&6.4	Size 3	-12.29	0.00	Significant
	Size 4	-6.44	0.00	Significant
1.6&3.2	Size 3	-2.04	0.08	Not significant
	Size 4	-2.98	0.02	Significant
1.6&6.4	Size 3	-7.99	0.00	Significant
	Size 4	-8.91	0.00	Significant
3.2&6.4	Size 3	-1.16	0.27	Not significant
	Size 4	2.30	0.05	Not significant

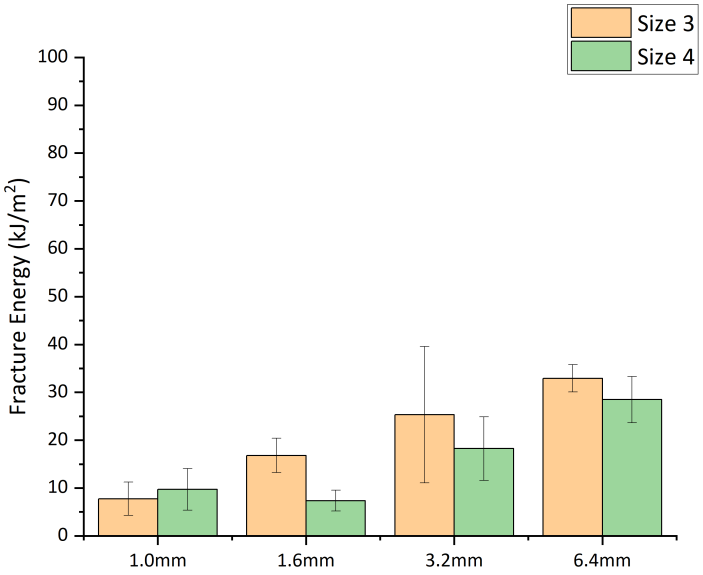

Figure 31. Fracture energy of DFC panels under 4 thicknesses

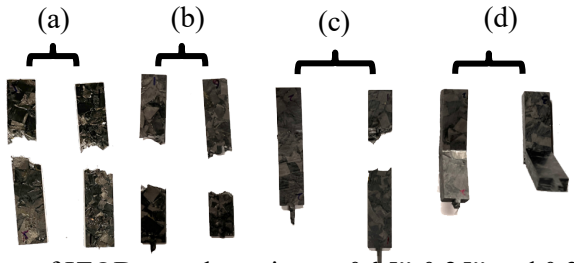

Figure 32. Comparison of IZOD tested specimens 0.25”-0.25” and 0.25”-0.125” with (a) 1.0mm; (b) 1.6mm; (c) 3.2mm; (d) 6.4mm thickness, respectively

6.1.3.1. Optical Microscope Investigation

The failure cross-section of IZOD coupon was detected by optical microscope and one

coupon from Sample 1was shown in Figure 33. In general, the surface of coupon clearly showed some poor resin region happened and the shape of flakes could be clearly identified except the orientation of flakes. According to (a) and (b), the failure happened from tension side is primarily caused by matrix failure due to the closely transverse flakes. From compression side, fibers were clearly pulled out which was heavily impacted by flake stacking and the interface between flakes were bonded by resin. Intrinsic flaws such the gap between flakes could cause poor resin region or rich resin region. In general, fiber breakage was not significant by analyzing failure cross-section and the primary failure happened was matrix failure.

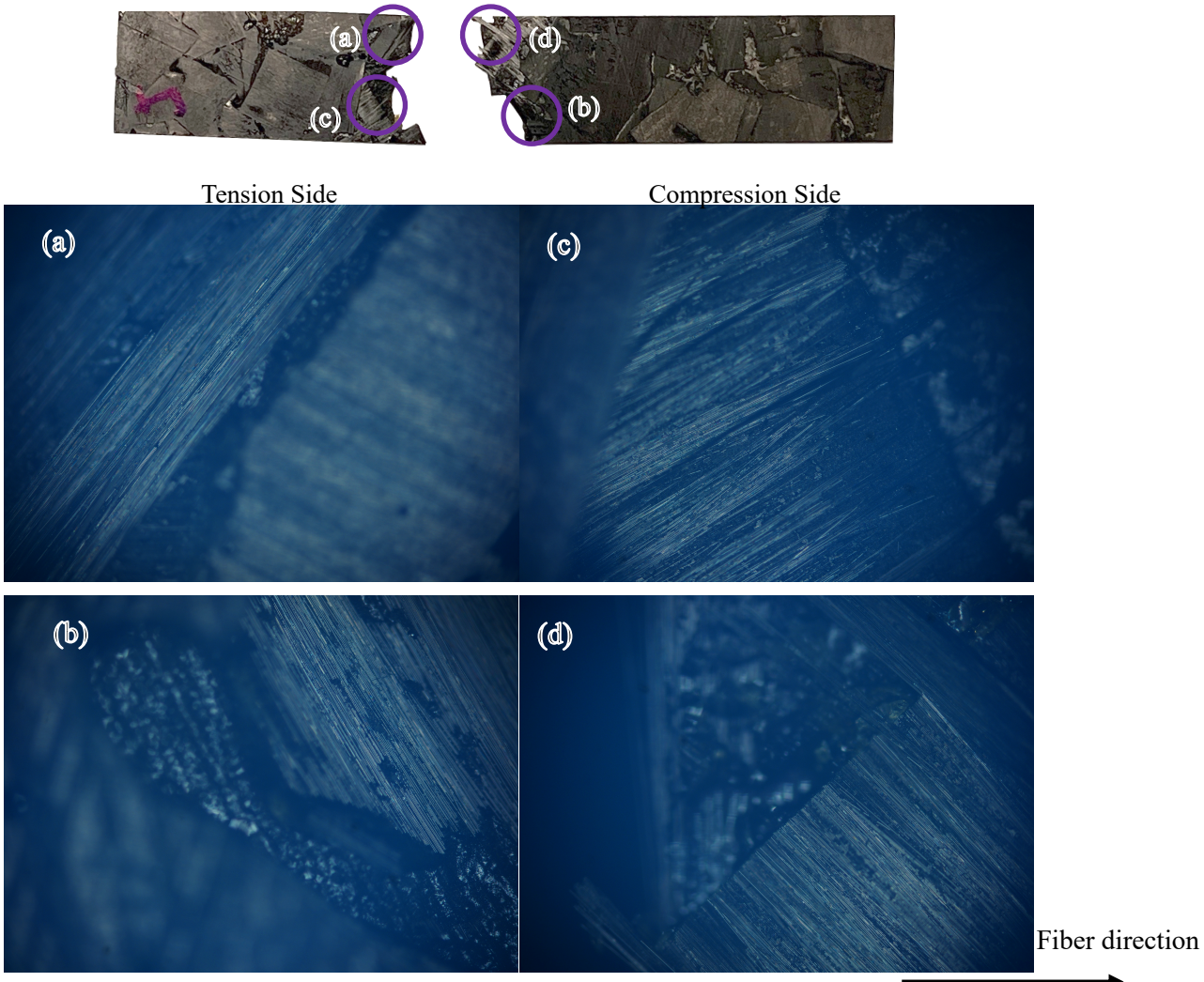

Figure 33. Performance of failure cross-section, (a) and (b) are Tension sides; (c) and (d) are Compression sides

6.1.3.2. Regression Analysis

Compared IZOD regression results to tensile regression results, panels made of 0.125" flake length had a higher R^2 by linear regression which showed a strong linear correlation between impact energy and thickness. After introduced one more order, both types of panel had higher correlations, both were close to 1 not as overfitting at the third polynomial regression.

According to GPR results from four different kernels presented by Figure 34, the highest predictive impact energy located from thickness of 4 to 8mm. The trend of decrease could be defined by a parameter after 6.4mm which was relative to the processing defects caused by water-jet cutting.

Table 15. Regression results of IZOD test

Regression Method	**R^2 for Size 3**	**R^2 for Size 4**
Linear	0.86	0.94
Secondary Polynomial	0.97	0.95
Third Polynomial	1.00	1.00

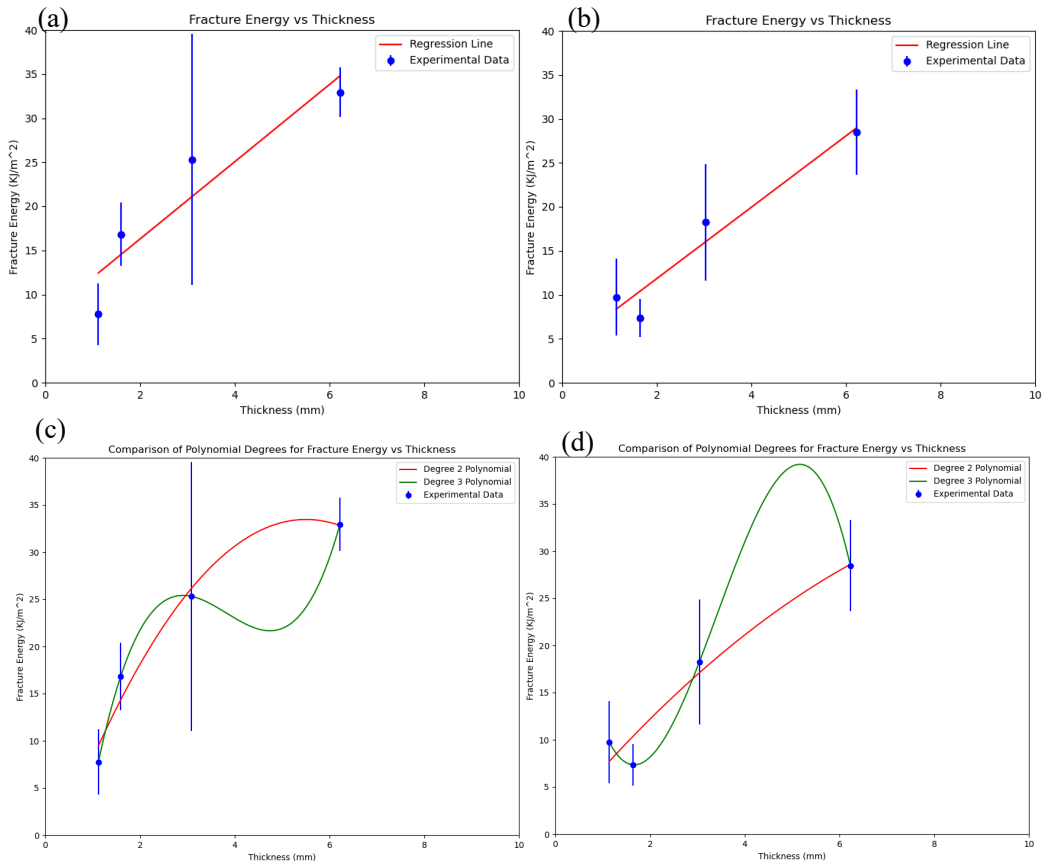

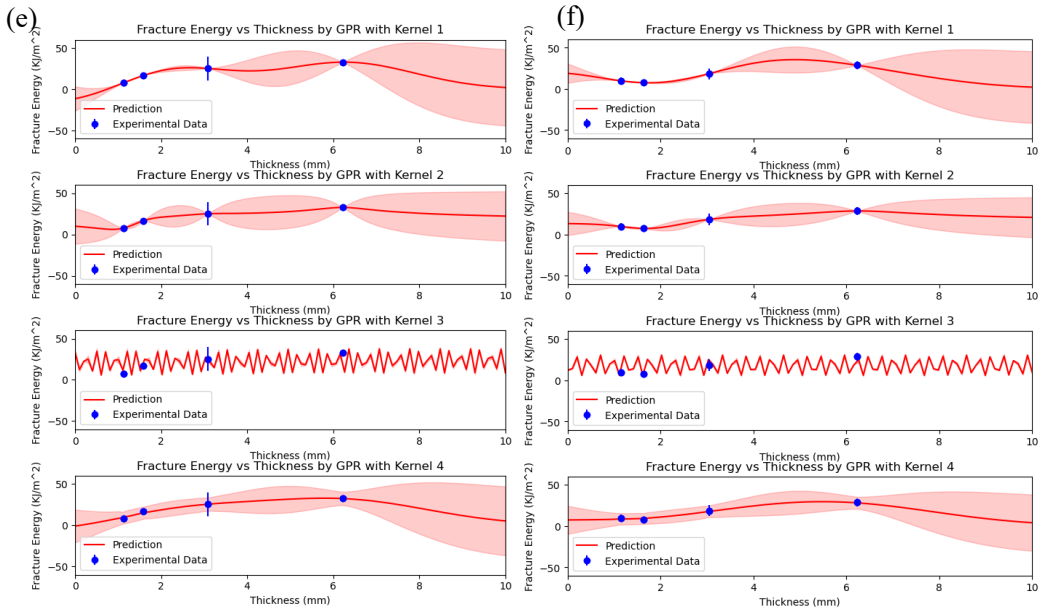

Figure 34. Different Regression results for two sizes of flakes

6.2. PART 2: rBMC

6.2.1. Thermal Properties Analysis of rBMC

To investigate the thermal behavior of EP-YDF-173, DSC and TGA were used under the same steps as below. The first endothermic peak was shown around -10C which could be performed as glass transition happens with temperature increase. For the new epoxy system, the curing process started at about 161C and the highest curing rate was at 225C. The range of curing temperature was shown from 161C to 300C, and further degradation of resin was happening after 300C.

The actual volume content of resin could be tested by TGA. The ideal conditions could be assumed as the carbon fibers cannot impact the degradation kinetics of epoxy resin system; the weight of carbon fiber remains no changes. To calibrate and validate actual value, virgin prepreg was tested by TGA with two atmospheres, nitrogen, and air. The validated volume content of resin in virgin prepreg was 45.12%, actual values could be normalized by reduce 0.31%. Figure 36 presented actual volume content of resin by TGA. Except size 1 and size 2, the TGA data for other sizes was only off by 2-3%. For long flakes, their dispersion was not good so that the resin content of each part was uneven, resulting in a large difference between desired value.

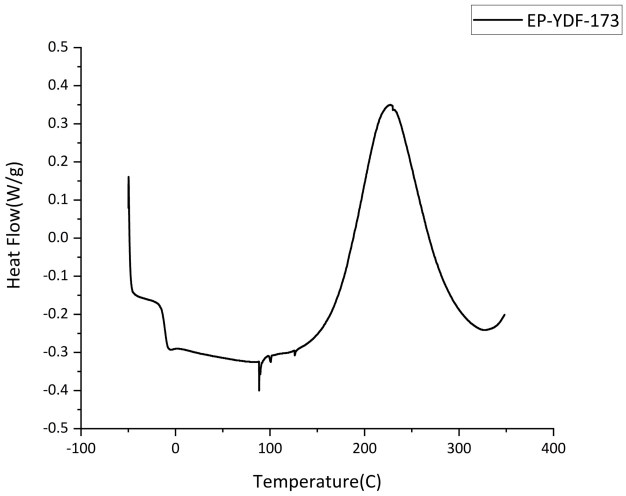

Figure 35. DSC plot for EP-YDF-173

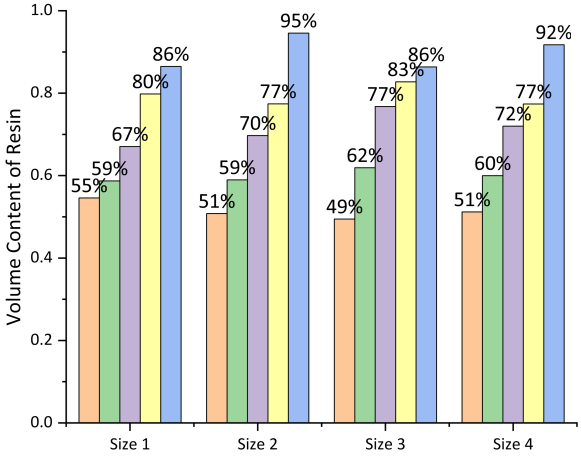

Figure 36. TGA results

6.2.2. IZOD Test

Four different formulas of rBMC were characterized by IZOD impact tests and results were presented by Table 16 to 19 and visualized by Figure 37. The chart clearly shows that the larger the flake size, the higher the fracture energy about 57.68 ± 8.75 KJ/m^2, indicating the stronger the fracture resistance. With the increase of volume content of resin value (from 50% to 90%), the fracture energy decreases, indicating that the material can absorb less energy at higher resin content. The error bars represent the variability of the data, with the great variability observed in Size 1 and Size 2. Since the two flakes were not well dispersed in the additional resin, the mechanical properties

of each sample presented after hot pressing were different. A drop in Size 1 group at 60% was quite due to inhomogeneous distribution of fibers. According to figure 38, the section view showed that 50% of the samples had more fibers to resist the impact of splitting, while 60% of the samples had transverse and laterally inclined fibers.

In addition, the reason for the drop in impact resistance could be residual stress in the Size 1 and Size 2 samples. Higher resin content can lead to PID which were shown in figure 18 due to the inhomogeneous distribution of rBMC. Ideally, fibers are evenly distributed in the resin to maintain the panel's structural stability and flatness. With the resin content increase, resin-rich areas may form between the fibers. These areas can experience uneven shrinkage during the curing process, resulting in the warping of the panels [102].

Depending on table 18, Size 3 showed a considerable dispersion of fibers and compared to DFC 3.2mm samples with virgin resin content, rBMC showed better fracture energy absorption by recombining the dispersed fiber resin increased by 110% at 50% volume content of resin rBMC.

The lowest impact resistance was shown by Size 4 with 90% resin content, dropped about 90.52% compared with the highest fracture energy value, which was due longer fiber provides strong interfacial bonding between fiber and matrix and transfers more energy to prevent fibers pulling out [112, 113]. Short fibers have a higher surface to volume ratio, resulting in an increased interface area with the resin and the mechanical properties of composites depend more on the fiber-resin interface than the resin content [114]. In composites with very short fibers, the properties of the resin may start to dominate over the properties contributed by the fibers, particularly if the fibers are not able to effectively transfer load due to poor bonding or alignment [115].

The failure comparison of specimens was shown in figure 39, significant failure was shown in Size 1 and Size 2 groups, visible transverse flakes separation was clearly presented at failure position. On the other hand, the partial crack failure was due to longitudinal fibers distributing at failure position. Unlike Size 1 and Size 2, the higher volume content of resin in Size 3 and the fracture of Size 4 are more orderly, and the fracture mode can be seen as fiber fracture and matrix failure.

Table 16. IZOD test results for rBMC Size 1

Volume content of resin	cross section area e-5 m^2	±std e-7	Fracture Energy KJ/m^2	±std	Failure Type
50%	4.24	2.98	57.68	8.75	P
60%	4.33	1.95	15.68	7.24	C
70%	3.98	7.48	24.68	13.80	C
80%	3.88	10.57	39.87	21.18	C
90%	4.18	3.19	12.57	14.62	C

Table 17. IZOD test results for rBMC Size 2

Volume content of resin	cross section area e-5 m^2	±std e-7	Fracture Energy KJ/m^2	±std	Failure Type
50%	3.99	6.76	39.49	9.88	P
60%	3.64	5.66	33.02	14.03	P
70%	3.99	13.65	18.05	9.22	C
80%	4.19	1.26	11.87	2.54	C
90%	4.08	9.33	9.83	2.47	C

Table 18. IZOD test results for rBMC Size 3

Volume content of resin	cross section area e-5 m^2	±std e-7	Fracture Energy KJ/m^2	±std	Failure Type
44.81%	3.67	27.13	25.31	14.24	P
50%	4.37	4.12	52.97	12.89	P
60%	4.30	8.35	47.81	13.80	C
75%	3.69	9.95	33.17	16.10	C
80%	3.79	12.16	15.39	7.42	C
90%	4.13	7.63	9.39	5.16	C

Table 19. IZOD test results for rBMC Size 4

Volume content of resin	cross section area e-5 m^2	±std e-7	Fracture Energy KJ/m^2	±std	Failure Type
44.81%	3.60	29.57	18.24	6.64	C
50%	4.09	4.67	13.39	3.36	C
60%	4.25	14.65	15.08	9.50	C
70%	4.06	3.56	13.21	6.21	C
80%	3.85	1.91	13.45	4.79	C
90%	4.09	10.44	5.47	0.62	C

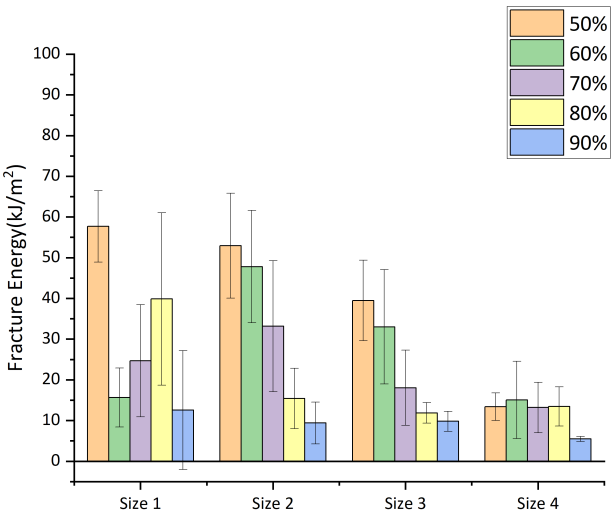

Figure 37. IZOD test results for rBMC

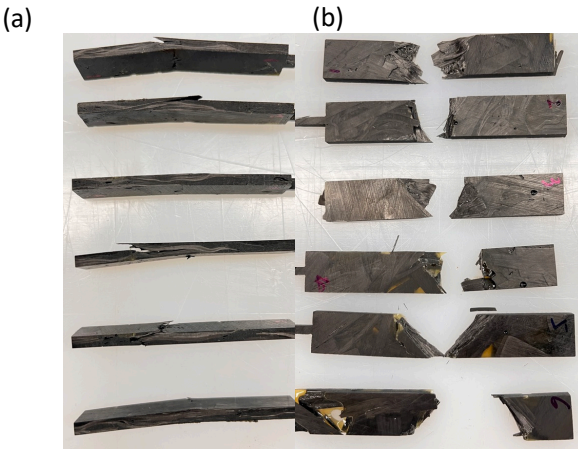

Figure 38. Size 1 IZOD sample comparison (a) 50%; (b) 60%

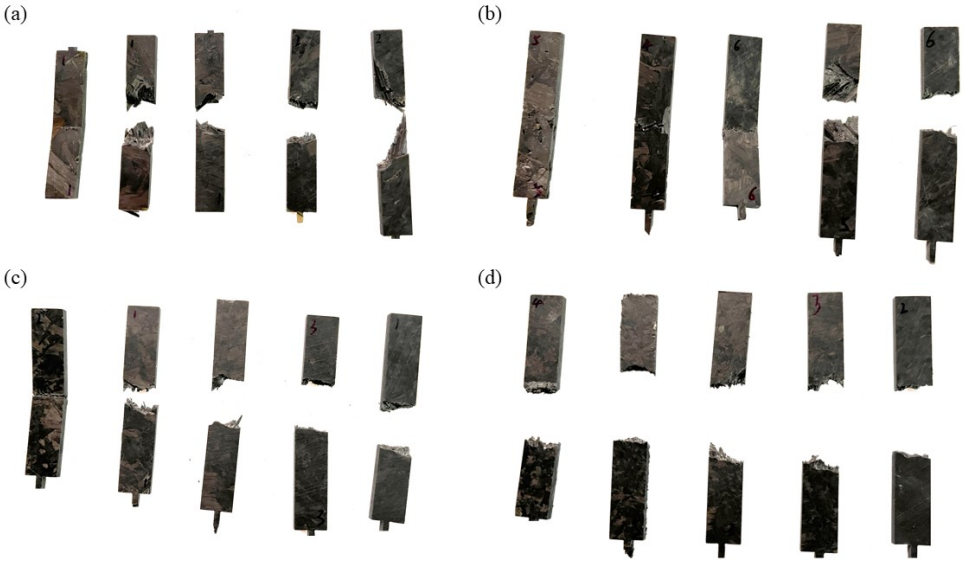

Figure 39. IZOD sample comparison (a) Size 1; (b) Size 2; (c) Size 3; (d) Size 4 in the order of 50%, 60%, 70%, 80%, 90%

6.2.3. Optimized Model by Gaussian Process Regression (GPR)

To generate a dataset based on experimental points and consider GPR results from DFC section, RBF as a high-performance kernel was setup. A predict ML model was built relative to fracture energy and volume content of resin.

(a) With the volume content of resin increased to about 45%, the fracture energy reached a peak, and then with the increase of resin content to about 60%, the fracture energy gradually decreased to the lowest point. After that, when the resin content continued to increase to about 65%, the fracture energy rose slightly, and finally stabilized between 80% and 100% and slightly decreased. In the whole range of resin content, the change of fracture energy showed a certain fluctuation, which may reflect the influence of the difference of the internal structure of the material under different resin content on its mechanical properties.

(b) GPR prediction for Size 2 showed a downward trend in fracture energy as the resin content increases, starting from a high point of about 50 KJ/m². The experimental data points are tightly clustered, following a similar trend that was often well captured by GPR models. As the resin content increases, the confidence interval widened slightly, indicating increased uncertainty in the model's predictions.

(c) With the increase of resin content, the fracture energy initially increased slightly, reached a small peak (around 50%), and then showed a downward trend, especially after 55%, the fracture energy decreased significantly, and maintained a relatively stable trend in the range of 60% to 100%.

(d) The curve predicted by GPR was smoother, showing a slight decrease in fracture energy as the resin content increases. The predicted curve gradually decreased from left to right, but the overall change was little, indicating that the change of resin content had a relatively limited effect on the fracture energy.

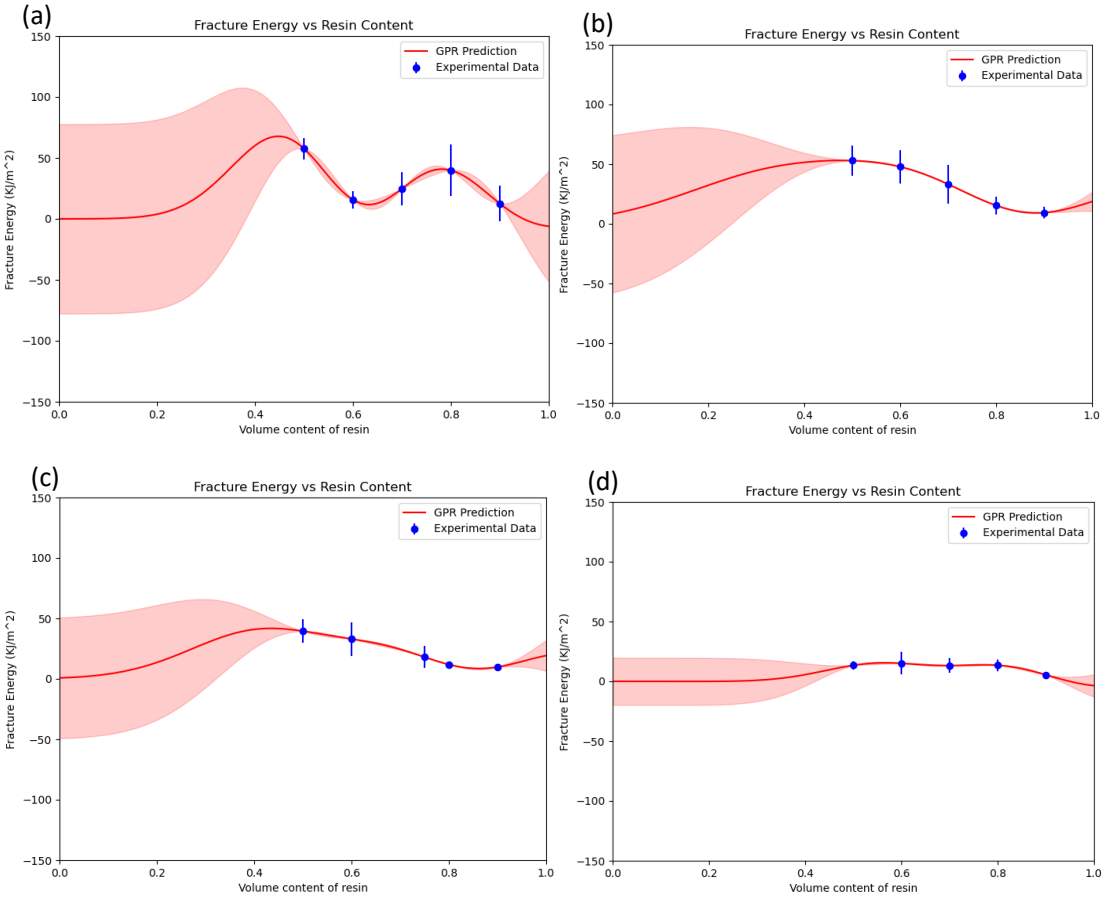

Figure 40. IZOD GPR prediction (a) Size 1; (b) Size 2; (c) Size 3; (d) Size 4

7. CONCLUSION

As an effective and convenient method, DFC and rBMC played an important role in recycling uncured prepreg scraps. For DFC materials, flake prepregs were difficult to disperse evenly, resulting in flake accumulation and gaps between ends of flakes, resulting in internal structural defects. Compared 0.25”-0.25” to 0.25”-0.125” panels, the longer flake usually had better mechanical properties, which performed higher about 10MPa tensile strength and 10KJ impact energy per meter area except the uncertainty caused by the random distribution of flake when the thickness was thin, and the defects caused by sample processing. CNN as a powerful method was used for object detection and the model showed a considerable result which could be optimized by increasing the model size. As a prediction model based on a small number of data points, GPR provided a wide range of prediction results for optimizing manufacturing parameters. Considering the defects caused by processing at 6.4mm, the maximum

mechanical property was between 3-6mm in the thickness range.

rBMC as a new recycling method breaks down the prepreg's structure, the state of the dispersed single fiber was proportional to the flake length and the volume of additional resin added. With the volume content of resin increase and length of flake decrease, the degree of dispersion of fibers was improved.

In rBMC, the longer flakes could provide higher mechanical properties but the strength of each part was inhomogeneous due to poor dispersion. In addition, because of the poor interfacial bonding between the shorter fibers and the resin, the fibers played a small role in the composites. Based on the above, Size 3 was a good option, the dispersion of impact resistance results was minor, and the strength could reach a maximum of 40KJ/m^2 when the resin volume fraction was around 50%.

8. FURTHER WORK

For the current prediction model, you can continue to optimize the model by producing data points that are higher in the forecast results. For rBMC, this recycling method involves different manufacturing parameters, such as the hot-pressing pressure, the type of resin added, the blending time, and other production parameters can be used as optimization parameters. In addition, this experiment costs a lot from manufacturing to characterization, so the cross validation for simulation and experiment is an optimal solution.

REFERENCES

[1] G. Nilakantan and S. Nutt, "Reuse and upcycling of thermoset prepreg scrap: Case study with out-of-autoclave carbon fiber/epoxy prepreg," vol. 52, no. 3, pp. 341-360, 2018.

[2] I. Okajima, K. Watanabe, S. Haramiishi, M. Nakamura, Y. Shimamura, and T. Sako, "Recycling of carbon fiber reinforced plastic containing amine-cured epoxy resin using supercritical and subcritical fluids," *The Journal of supercritical fluids,* vol. 119, pp. 44-51, 2017.

[3] C. Yaw Attahu, C. Ket Thein, K. H. Wong, and J. Yang, "Enhanced damping and stiffness trade-off of composite laminates interleaved with recycled carbon fiber and short virgin aramid fiber non-woven mats," *Composite structures,* vol. 297, p. 115981, 2022.

[4] S. Ko *et al.*, *Computational Investigation of the Stochastic Tensile Behavior of Discontinuous Fiber Composite Structures*. 2022.

[5] D. Gay, *Composite Materials : Design and Applications, Third Edition*, 3rd ed. ed. Bosa Roca : CRC Press LLC, 2014.

[6] C. S. R. de Souza *et al.*, "Reuse of Uncured Carbon Fiber/Epoxy Resin Prepreg Scraps: Mechanical Behavior and Environmental Response," *ACS Sustainable Chemistry & Engineering,* vol. 7, no. 2, pp. 2200-2206, 2019/01/22 2019.

[7] N. van de Werken, H. Tekinalp, P. Khanbolouki, S. Ozcan, A. Williams, and M. Tehrani, "Additively manufactured carbon fiber-reinforced composites: State of the art and perspective," *Additive Manufacturing,* vol. 31, p. 100962, 2020/01/01/ 2020.

[8] D. Borjan, Ž. Knez, and M. Knez, "Recycling of Carbon Fiber-Reinforced Composites—Difficulties and Future Perspectives," *Materials,* vol. 14, no. 15, p. 4191, 2021.

[9] J. A. Butenegro, M. Bahrami, J. Abenojar, and M. Á. Martínez, "Recent Progress in Carbon Fiber Reinforced Polymers Recycling: A Review of Recycling Methods and Reuse of Carbon Fibers," *Materials,* vol. 14, no. 21, p. 6401, 2021.

[10] E. J. Barbero, *Introduction to Composite Materials Design*, 3rd ed. ed. Milton : CRC Press LLC, 2017.

[11] D. Abliz, D. Yugang, L. Steuernagel, X. I. E. Lei, L. I. Dichen, and G. Ziegmann, "Curing Methods for Advanced Polymer Composites - A Review," *Polymers & polymer composites,* vol. 21, no. 6, pp. 341-348, 2013.

[12] P. Baumli, J. Sychev, I. Budai, J. Szabo, and G. Kaptay, "Fabrication of carbon fiber reinforced aluminum matrix composites via a titanium-ion containing flux," *Composites Part A: Applied Science and Manufacturing,* vol. 44, pp. 47-50, 2013.

[13] J. Sun, S. Yu, J. Wade-Zhu, X. Chen, J. Binner, and J. Bai, "3D printing of layered ceramic/carbon fiber composite with improved toughness," *Additive Manufacturing,* vol. 50, p. 102543, 2022/02/01/ 2022.

[14] R. O. Ebewele, *Polymer science and technology*. CRC press, 2000.

[15] B. A. Newcomb, "Processing, structure, and properties of carbon fibers," *Composites Part A: Applied Science and Manufacturing,* vol. 91, pp. 262-282, 2016/12/01/ 2016.

[16] D. Chu, W. Bai, Y. He, M. Ye, and J. Li, "Research on Lightweight Technology of new carbon fiber wheel hub structure," in *IOP Conference Series: Earth and Environmental Science*, 2021, vol. 632, no. 5, p. 052071: IOP Publishing.

[17] A. Gupta, D. Paliwal, and P. J. J. o. M. S. Bajaj, Part C: Polymer Reviews, "Acrylic precursors for carbon fibers," vol. 31, no. 1, pp. 1-89, 1991.

[18] D. Edie, R. J. C.-c. m. Diefendorf, and composites, "Carbon fiber manufacturing," pp. 19-37,

1993.

[19] G. G. J. C. Tibbetts, "Vapor-grown carbon fibers: status and prospects," vol. 27, no. 5, pp. 745-747, 1989.

[20] P. K. Mallick, *Fiber-Reinforced Composites : Materials, Manufacturing, and Design, Third Edition*, 3rd ed. ed. Bosa Roca : CRC Press LLC, 2007.

[21] W. Zhao, B. Li, M. Xu, K. Yang, and L. Lin, "Novel intumescent flame retardants: synthesis and application in polycarbonate: NOVEL INTUMESCENT FLAME RETARDANTS," *Fire and materials,* vol. 37, no. 7, pp. 530-546, 2013.

[22] D. Lukkassen and A. J. N. U. C. Meidell, Hin, "Advanced materials and structures and their fabrication processes," 2003.

[23] Q. Guo, *Thermosets: structure, properties, and applications*. Woodhead Publishing, 2017.

[24] H. Q. Pham and M. J. J. U. s. E. o. I. C. Marks, "Epoxy resins," 2000.

[25] C. A. Navarro, C. R. Giffin, B. Zhang, Z. Yu, S. R. Nutt, and T. J. Williams, "A structural chemistry look at composites recycling," *Materials horizons,* vol. 7, no. 1, pp. 2479-2486, 2020.

[26] Y. Yang, R. Boom, B. Irion, D.-J. van Heerden, P. Kuiper, and H. de Wit, "Recycling of composite materials," *Chemical Engineering and Processing: Process Intensification,* vol. 51, pp. 53-68, 2012/01/01/ 2012.

[27] C. Xiong, Q. Li, T. Lan, H. Li, W. Long, and F. Xing, "Sustainable use of recycled carbon fiber reinforced polymer and crumb rubber in concrete: mechanical properties and ecological evaluation," *Journal of cleaner production,* vol. 279, p. 123624, 2021.

[28] J. Howarth, S. S. R. Mareddy, and P. T. Mativenga, "Energy intensity and environmental analysis of mechanical recycling of carbon fibre composite," *Journal of cleaner production,* vol. 81, pp. 46-50, 2014.

[29] A. Vo Dong, C. Azzaro-Pantel, and M. Boix, "A multi-period optimisation approach for deployment and optimal design of an aerospace CFRP waste management supply chain," *Waste Management,* vol. 95, pp. 201-216, 2019/07/15/ 2019.

[30] M. Okayasu, T. Yamazaki, K. Ota, K. Ogi, and T. Shiraishi, "Mechanical properties and failure characteristics of a recycled CFRP under tensile and cyclic loading," *International journal of fatigue,* vol. 55, pp. 257-267, 2013.

[31] T. Yamamoto, Y. Makino, and K. Uematsu, "Improved mechanical properties of PMMA composites: Dispersion, diffusion and surface adhesion of recycled carbon fiber fillers from CFRP with adsorbed particulate PMMA," *Advanced powder technology : the international journal of the Society of Powder Technology, Japan,* vol. 28, no. 10, pp. 2774-2778, 2017.

[32] M. Durante, L. Boccarusso, D. De Fazio, A. Formisano, and A. Langella, "Investigation on the Mechanical Recycling of Carbon Fiber-Reinforced Polymers by Peripheral Down-Milling," *Polymers,* vol. 15, no. 4, p. 854, 2023.

[33] A. Danish *et al.*, "Utilization of recycled carbon fiber reinforced polymer in cementitious composites: A critical review," *Journal of Building Engineering,* vol. 53, p. 104583, 2022.

[34] S. J. Pickering, "Recycling technologies for thermoset composite materials—current status," *Composites Part A: Applied Science and Manufacturing,* vol. 37, no. 8, pp. 1206-1215, 2006/08/01/ 2006.

[35] S. J. Pickering, R. M. Kelly, J. R. Kennerley, C. D. Rudd, and N. J. Fenwick, "A fluidised-bed process for the recovery of glass fibres from scrap thermoset composites," *Composites Science and Technology,* vol. 60, no. 4, pp. 509-523, 2000/03/01/ 2000.

[36] J. Qureshi, "A Review of Recycling Methods for Fibre Reinforced Polymer Composites," *Sustainability*, vol. 14, no. 24. doi: 10.3390/su142416855

[37] S. Karuppannan Gopalraj and T. Kärki, "A review on the recycling of waste carbon fibre/glass fibre-reinforced composites: fibre recovery, properties and life-cycle analysis," *SN Applied Sciences,* vol. 2, no. 3, p. 433, 2020/02/18 2020.

[38] E. Pakdel, S. Kashi, R. Varley, and X. Wang, "Recent progress in recycling carbon fibre reinforced composites and dry carbon fibre wastes," *Resources, Conservation and Recycling,* vol. 166, p. 105340, 2021/03/01/ 2021.

[39] A. Torres *et al.*, "Recycling by pyrolysis of thermoset composites: characteristics of the liquid and gaseous fuels obtained," *Fuel (Guildford),* vol. 79, no. 8, pp. 897-902, 2000.

[40] S. Hao, L. He, J. Liu, Y. Liu, C. Rudd, and X. Liu, "Recovery of Carbon Fibre from Waste Prepreg via Microwave Pyrolysis," *Polymers,* vol. 13, no. 8, p. 1231, 2021.

[41] L. O. Meyer, K. Schulte, and E. Grove-Nielsen, "CFRP-Recycling Following a Pyrolysis Route: Process Optimization and Potentials," *Journal of composite materials,* vol. 43, no. 9, pp. 1121-1132, 2009.

[42] J. Yang, J. Liu, W. Liu, J. Wang, and T. Tang, "Recycling of carbon fibre reinforced epoxy resin composites under various oxygen concentrations in nitrogen–oxygen atmosphere," *Journal of analytical and applied pyrolysis,* vol. 112, pp. 253-261, 2015.

[43] G. Jiang and S. J. Pickering, "Structure–property relationship of recycled carbon fibres revealed by pyrolysis recycling process," *Journal of materials science,* vol. 51, no. 4, pp. 1949-1958, 2015.

[44] G. Jiang, S. J. Pickering, E. H. Lester, T. A. Turner, K. H. Wong, and N. A. Warrior, "Characterisation of carbon fibres recycled from carbon fibre/epoxy resin composites using supercritical n-propanol," *Composites science and technology,* vol. 69, no. 2, pp. 192-198, 2009.

[45] G. Oliveux, L. O. Dandy, and G. A. Leeke, "Degradation of a model epoxy resin by solvolysis routes," *Polymer degradation and stability,* vol. 118, pp. 96-103, 2015.

[46] D. Braun, W. von Gentzkow, and A. P. Rudolf, "Hydrogenolytic degradation of thermosets," *Polymer Degradation and Stability,* vol. 74, no. 1, pp. 25-32, 2001/01/01/ 2001.

[47] H. Weingärtner and E. U. Franck, "Supercritical Water as a Solvent," vol. 44, no. 18, pp. 2672-2692, 2005.

[48] M. Goto, "Chemical recycling of plastics using sub- and supercritical fluids," *The Journal of Supercritical Fluids,* vol. 47, no. 3, pp. 500-507, 2009/01/01/ 2009.

[49] M. Mukhopadhyay, "Extraction and processing with supercritical fluids," vol. 84, no. 1, pp. 6-12, 2009.

[50] A. Loppinet-Serani, C. Aymonier, and F. Cansell, "Supercritical water for environmental technologies," vol. 85, no. 5, pp. 583-589, 2010.

[51] E. Reverchon and R. Adami, "Nanomaterials and supercritical fluids," *The Journal of Supercritical Fluids,* vol. 37, no. 1, pp. 1-22, 2006/02/01/ 2006.

[52] W. Su, H. Zhang, Y. Xing, X. Li, J. Wang, and C. Cai, "A Bibliometric Analysis and Review of Supercritical Fluids for the Synthesis of Nanomaterials," vol. 11, no. 2, p. 336, 2021.

[53] P. Anastas and N. Eghbali, "Green chemistry: principles and practice," *Chemical Society reviews,* vol. 39, no. 1, pp. 301-312, 2010.

[54] J. Jiang *et al.*, "On the successful chemical recycling of carbon fiber/epoxy resin composites under the mild condition," *Composites Science and Technology,* vol. 151, pp. 243-251, 2017/10/20/ 2017.

[55] Y. Wang *et al.*, "Chemical Recycling of Carbon Fiber Reinforced Epoxy Resin Composites via Selective Cleavage of the Carbon–Nitrogen Bond," *ACS Sustainable Chemistry & Engineering,* vol. 3, no. 12, pp. 3332-3337, 2015/12/07 2015.

[56] L. Yuyan, S. Guohua, and M. Linghui, "Recycling of carbon fibre reinforced composites using water in subcritical conditions," *Materials science & engineering. A, Structural materials : properties, microstructure and processing,* vol. 520, no. 1, pp. 179-183, 2009.

[57] P. Rajaee, F. Ashenai Ghasemi, M. Fasihi, and N. J. P. C. Amini, "Microstructural analysis and multi‐response optimization of mechanical properties of bulk molding compound," vol. 43, no. 1, pp. 593-607, 2022.

[58] M. Barczewski, D. Matykiewicz, J. Andrzejewski, and K. Skórczewska, "Application of waste bulk moulded composite (BMC) as a filler for isotactic polypropylene composites," *Journal of Advanced Research,* vol. 7, no. 3, pp. 373-380, 2016/05/01/ 2016.

[59] D. Matykiewicz, M. Barczewski, and T. Sterzyński, "Morphology and thermomechanical properties of epoxy composites highly filled with waste bulk molding compounds (BMC)," vol. 35, no. 8, pp. 805-811, 2015.

[60] J. M. Kenny and M. Opalicki, "Processing of short fibre/thermosetting matrix composites," *Composites Part A: Applied Science and Manufacturing,* vol. 27, no. 3, pp. 229-240, 1996/01/01/ 1996.

[61] L. J. I. C. I. Landis, "Structural thermoset compounds and their primary applications," 2016.

[62] A. K. Bledzki, H. Seidlitz, J. Krenz, K. Goracy, M. Urbaniak, and J. J. Rösch, "Recycling of Carbon Fiber Reinforced Composite Polymers-Review-Part 2: Recovery and Application of Recycled Carbon Fibers," *Polymers,* vol. 12, no. 12, p. 3003, 2020.

[63] K. M. Hurley, *The Effect of Recyclate Geometry on the Properties of Recycled Flake Reinforced Thermoset Composites*. University of Washington, 2012.

[64] C. Schoenholz and N. Zobeiry, "An Accelerated Process Optimization Method to Minimize Deformations in Composites Using Theory-guided Probabilistic Machine Learning," *Composites Part A: Applied Science and Manufacturing,* vol. 176, p. 107842, 2024/01/01/ 2024.

[65] M. Mohri, A. Rostamizadeh, and A. Talwalkar, *Foundations of machine learning*. MIT press, 2018.

[66] K. P. Murphy, *Probabilistic machine learning: an introduction*. MIT press, 2022.

[67] A. Le Glaz *et al.*, "Machine Learning and Natural Language Processing in Mental Health: Systematic Review," *J Med Internet Res,* vol. 23, no. 5, p. e15708, 2021/5/4 2021.

[68] S. Kumar and M. Zymbler, "A machine learning approach to analyze customer satisfaction from airline tweets," *Journal of Big Data,* vol. 6, no. 1, p. 62, 2019/07/17 2019.

[69] V. J. H. b. Nasteski, "An overview of the supervised machine learning methods," vol. 4, pp. 51-62, 2017.

[70] X. Su, X. Yan, and C. L. Tsai, "Linear regression," *Wiley Interdisciplinary Reviews: Computational Statistics,* vol. 4, no. 3, pp. 275-294, 2012.

[71] E. Ostertagová, "Modelling using Polynomial Regression," *Procedia Engineering,* vol. 48, pp. 500-506, 2012/01/01/ 2012.

[72] W. Krämer and H. Sonnberger, *The linear regression model under test*. Springer Science & Business Media, 2012.

[73] B. E. Boser, I. M. Guyon, and V. N. Vapnik, "A training algorithm for optimal margin classifiers," presented at the Proceedings of the fifth annual workshop on Computational learning theory,

Pittsburgh, Pennsylvania, USA, 1992. Available: https://doi.org/10.1145/130385.130401
[74] W. S. Noble, "What is a support vector machine?," *Nature Biotechnology,* vol. 24, no. 12, pp. 1565-1567, 2006/12/01 2006.
[75] M. A. Hearst, S. T. Dumais, E. Osuna, J. Platt, and B. Scholkopf, "Support vector machines," *IEEE Intelligent Systems and their Applications,* vol. 13, no. 4, pp. 18-28, 1998.
[76] S. Suthaharan, "Support Vector Machine," in *Machine Learning Models and Algorithms for Big Data Classification: Thinking with Examples for Effective Learning*, S. Suthaharan, Ed. Boston, MA: Springer US, 2016, pp. 207-235.
[77] S. Albawi, T. A. Mohammed, and S. Al-Zawi, "Understanding of a convolutional neural network," in *2017 international conference on engineering and technology (ICET)*, 2017, pp. 1-6: Ieee.
[78] K. O'shea and R. Nash, "An introduction to convolutional neural networks," *arXiv preprint arXiv:1511.08458,* 2015.
[79] H. H. Aghdam and E. J. Heravi, "Guide to convolutional neural networks," *New York, NY: Springer,* vol. 10, no. 978-973, p. 51, 2017.
[80] W. Sha *et al.*, "Machine learning in polymer informatics," *InfoMat,* vol. 3, no. 4, pp. 353-361, 2021.
[81] J. J. a. p. a. Wang, "An intuitive tutorial to Gaussian processes regression," 2020.
[82] E. Schulz, M. Speekenbrink, and A. Krause, "A tutorial on Gaussian process regression: Modelling, exploring, and exploiting functions," *Journal of Mathematical Psychology,* vol. 85, pp. 1-16, 2018.
[83] S. T. Ounpraseuth, "Gaussian processes for machine learning," ed: Taylor & Francis, 2008.
[84] D. J. U. h. w. c. t. e. d. c. Duvenaud, "The kernel cookbook: Advice on covariance functions," 2014.
[85] M. J. I. j. o. n. s. Seeger, "Gaussian processes for machine learning," vol. 14, no. 02, pp. 69-106, 2004.
[86] M. J. a. p. a. Ebden, "Gaussian processes: A quick introduction," 2015.
[87] T. Hida and M. Hitsuda, *Gaussian processes*. American Mathematical Soc., 1993.
[88] C. B. J. S. N. Do, Lecture on Machine Learning, CS, "The multivariate Gaussian distribution," vol. 229, 2008.
[89] J. Joyce, "Bayes' theorem," 2003.
[90] D. J. E. o. b. Berrar and c. b. A. o. bioinformatics, "Bayes' theorem and naive Bayes classifier," vol. 403, p. 412, 2018.
[91] M. Bédard, D. A. Fraser, and A. Wong, "Higher accuracy for Bayesian and frequentist inference: Large sample theory for small sample likelihood," 2007.
[92] T. Hastie *et al.*, "Unsupervised learning," pp. 485-585, 2009.
[93] M. Usama *et al.*, "Unsupervised Machine Learning for Networking: Techniques, Applications and Research Challenges," *IEEE Access,* vol. 7, pp. 65579-65615, 2019.
[94] R. Bro and A. K. J. A. m. Smilde, "Principal component analysis," vol. 6, no. 9, pp. 2812-2831, 2014.
[95] U. Demšar, P. Harris, C. Brunsdon, A. S. Fotheringham, and S. McLoone, "Principal Component Analysis on Spatial Data: An Overview," *Annals of the Association of American Geographers,* vol. 103, no. 1, pp. 106-128, 2013/01/01 2013.
[96] A. Mansouri Tehrani *et al.*, "Machine learning directed search for ultraincompressible,

superhard materials," vol. 140, no. 31, pp. 9844-9853, 2018.

[97] C.-T. Chen and G. X. Gu, "Machine learning for composite materials," *MRS Communications,* vol. 9, no. 2, pp. 556-566, 2019.

[98] A. Eskandariyun *et al.*, "A Combined Finite Element and Machine Learning Approach to Accelerate Calibration and Validation of Numerical Models for Prediction of Failure in Aerospace Composite Parts," in *ASME 2023 Aerospace Structures, Structural Dynamics, and Materials Conference*, 2023, vol. ASME 2023 Aerospace Structures, Structural Dynamics, and Materials Conference, V001T01A013.

[99] Y. Wang, J. M. Lamim Ribeiro, and P. Tiwary, "Machine learning approaches for analyzing and enhancing molecular dynamics simulations," *Current Opinion in Structural Biology,* vol. 61, pp. 139-145, 2020/04/01/ 2020.

[100] E. M. Petrie, "Epoxy adhesive formulations," *(No Title),* 2006.

[101] M. A. Umarfarooq, P. S. Shivakumar Gouda, G. B. Veeresh kumar, N. R. Banapurmath, and A. Edacherian, "Impact of process induced residual stresses on interlaminar fracture toughness in carbon epoxy composites," *Composites Part A: Applied Science and Manufacturing,* vol. 127, p. 105652, 2019/12/01/ 2019.

[102] C. Zhang, G. Zhang, J. Xu, X. P. Shi, and X. Wang, "Review of curing deformation control methods for carbon fiber reinforced resin composites," *Polymer Composites,* vol. 43, no. 6, pp. 3350-3370, 2022.

[103] A. International, *Standard test method for tensile properties of plastics*. ASTM international, 2014.

[104] A. Greco, A. Maffezzoli, G. Buccoliero, F. Caretto, and G. Cornacchia, "Thermal and chemical treatments of recycled carbon fibres for improved adhesion to polymeric matrix," *Journal of composite materials,* vol. 47, no. 3, pp. 369-377, 2013.

[105] P. D. Soden, M. J. Hinton, and A. Kaddour, "Lamina properties, lay-up configurations and loading conditions for a range of fibre reinforced composite laminates," in *Failure criteria in fibre-reinforced-polymer composites*: Elsevier, 2004, pp. 30-51.

[106] M. R. Piggott, "Mesostructures and their mechanics in fibre composites," *Advanced Composite Materials,* vol. 6, no. 1, pp. 75-81, 1996/01/01 1996.

[107] K. Johanson, L. Harper, M. S. Johnson, and N. Warrior, "Heterogeneity of discontinuous carbon fibre composites: Damage initiation captured by Digital Image Correlation," *Composites Part A: Applied Science and Manufacturing,* vol. 68, pp. 304-312, 2015.

[108] S. Sultana, A. Asadi, J. Colton, and K. Kalaitzidou, "Composites made from CF prepreg trim waste tapes using sheet molding compounds (SMC) technology: Challenges and potential," *Composites Part A: Applied Science and Manufacturing,* vol. 134, p. 105906, 2020.

[109] W. Liu *et al.*, "Ssd: Single shot multibox detector," in *Computer Vision–ECCV 2016: 14th European Conference, Amsterdam, The Netherlands, October 11–14, 2016, Proceedings, Part I 14*, 2016, pp. 21-37: Springer.

[110] D. Patel, F. Patel, S. Patel, N. Patel, D. Shah, and V. Patel, "Garbage detection using advanced object detection techniques," in *2021 International Conference on Artificial Intelligence and Smart Systems (ICAIS)*, 2021, pp. 526-531: IEEE.

[111] A. B. Irez and H. Yakar, "Transformation of waste carbon fiber prepreg into sustainable composites: Application in the automotive industry components," *Polymer Composites,* 2024.

[112] P. B. Anand, A. Lakshmikanthan, M. P. Gowdru Chandrashekarappa, C. P. Selvan, D. Y. Pimenov,

and K. Giasin, "Experimental Investigation of Effect of Fiber Length on Mechanical, Wear, and Morphological Behavior of Silane-Treated Pineapple Leaf Fiber Reinforced Polymer Composites," vol. 10, no. 7, p. 56, 2022.

[113] Q. Yuan, D. Wu, J. Gotama, and S. Bateman, "Wood Fiber Reinforced Polyethylene and Polypropylene Composites with High Modulus and Impact Strength," vol. 21, no. 3, pp. 195-208, 2008.

[114] M. Z. Rong, M. Q. Zhang, Y. Liu, G. C. Yang, and H. M. Zeng, "The effect of fiber treatment on the mechanical properties of unidirectional sisal-reinforced epoxy composites," *Composites Science and Technology,* vol. 61, no. 10, pp. 1437-1447, 2001/08/01/ 2001.

[115] Y. Zhou, M. Fan, and L. J. C. P. B. E. Chen, "Interface and bonding mechanisms of plant fibre composites: An overview," vol. 101, pp. 31-45, 2016.